Birkbeck
UNIVERSITY OF LONDON

BIROn - Birkbeck Institutional Research Online

Alexander, Louise and Snape, J.F. and Joy, K.H. and Downes, Hilary and Crawford, Ian (2016) An analysis of Apollo lunar soil samples 12070,889, 12030,187 and 12070,891: basaltic diversity at the Apollo 12 landing site and implications for classification of small-sized lunar samples. Meteoritics & Planetary Science 51 (9), pp. 1654-1677. ISSN 1086-9379.

Downloaded from: https://eprints.bbk.ac.uk/id/eprint/15454/

Usage Guidelines:
Please refer to usage guidelines at https://eprints.bbk.ac.uk/policies.html or alternatively contact lib-eprints@bbk.ac.uk.

The Meteoritical Society

Meteoritics & Planetary Science 1–24 (2016)
doi: 10.1111/maps.12689

An analysis of Apollo lunar soil samples 12070,889, 12030,187, and 12070,891: Basaltic diversity at the Apollo 12 landing site and implications for classification of small-sized lunar samples

Louise ALEXANDER[1,2,*], Joshua F. SNAPE[2,3], Katherine H. JOY[4], Hilary DOWNES[1,2], and Ian A. CRAWFORD[1,2]

[1]Department of Earth and Planetary Science, Birkbeck College, University of London, Malet Street, London WC1E 7HX, UK
[2]The Centre for Planetary Sciences at UCL-Birkbeck, Gower Street, London WC1E 6BT, UK
[3]Department of Geosciences, Swedish Museum of Natural History, SE-104 05 Stockholm, Sweden
[4]School of Earth, Atmospheric and Environmental Sciences, University of Manchester, Oxford Road, Manchester M13 9PL, UK
*Corresponding author. E-mail: l.alexander@bbk.ac.uk

(Received 02 October 2015; revision accepted 06 June 2016)

Abstract–Lunar mare basalts provide insights into the compositional diversity of the Moon's interior. Basalt fragments from the lunar regolith can potentially sample lava flows from regions of the Moon not previously visited, thus, increasing our understanding of lunar geological evolution. As part of a study of basaltic diversity at the Apollo 12 landing site, detailed petrological and geochemical data are provided here for 13 basaltic chips. In addition to bulk chemistry, we have analyzed the major, minor, and trace element chemistry of mineral phases which highlight differences between basalt groups. Where samples contain olivine, the equilibrium parent melt magnesium number (Mg#; atomic Mg/[Mg + Fe]) can be calculated to estimate parent melt composition. Ilmenite and plagioclase chemistry can also determine differences between basalt groups. We conclude that samples of approximately 1–2 mm in size can be categorized provided that appropriate mineral phases (olivine, plagioclase, and ilmenite) are present. Where samples are fine-grained (grain size <0.3 mm), a "paired samples *t*-test" can provide a statistical comparison between a particular sample and known lunar basalts. Of the fragments analyzed here, three are found to belong to each of the previously identified olivine and ilmenite basalt suites, four to the pigeonite basalt suite, one is an olivine cumulate, and two could not be categorized because of their coarse grain sizes and lack of appropriate mineral phases. Our approach introduces methods that can be used to investigate small sample sizes (i.e., fines) from future sample return missions to investigate lava flow diversity and petrological significance.

INTRODUCTION

Mare basalt samples provide us with information on the composition of the Moon's upper mantle and partial melting history (e.g., Neal et al. 1994a, 1994b; Snyder et al. 1997; Shearer et al. 2006; Hallis et al. 2014). By examining the petrology and geochemistry of lunar basalts, and dating the samples studied (e.g., Nyquist and Shih 1992), we can learn about the composition and heterogeneity of the lunar mantle, and the evolution of lunar volcanism over time. This in turn provides important context for understanding wider magmatic and volcanic processes on other rocky planetary bodies (Basaltic Volcanism Study Project 1981).

In this paper, as part of a wider study examining basaltic diversity at the Apollo 12 landing site in Oceanus Procellarum (Crawford et al. 2007; Alexander et al. 2014; Snape et al. 2014), we present new detailed petrological and geochemical analyses for 13 coarse fines (approximately 2 mm in diameter) from Apollo 12 soil samples 12070,889, 12070,891, and 12030,187 (see Supplementary Note 2 in supporting information). Sample 12030,187 consists of a single basaltic fragment

© The Meteoritical Society, 2016.

(2.4 × 2.3 mm) sourced from an immature soil sample (maturity index Is/FeO = 14: Morris 1978), which is mainly composed of pale breccia fragments, possibly from a large breccia outcrop in the vicinity (McKay et al. 1971). This soil sample was collected near Head crater (see Supplementary Note 1 in supporting information), but the exact collection location is not known (Meyer 2011). The fines from 12070 form part of the contingency sample collected by the astronauts in front of the lunar module (Meyer 2011). Sample 12070 is a submature soil (Is/FeO = 47; Morris 1978). It consists of glazed aggregates (glass-bonded agglutinates) (26%), single crystals (16%), glasses (36%), rock fragments (7%), breccia fragments (7%), and spherules (1.2%) (McKay et al. 1971).

For reasons outlined by Crawford et al. (2007), a major part of our project was to identify basaltic fragments in the Apollo 12 regolith that may be exotic to the site, and possibly sourced from as yet unsampled younger basalts farther west in Oceanus Procellarum. To this end, we measured the bulk chemistry, modal mineralogy, mineral chemistry, and crystallization trends of the samples in an attempt to identify any that may not have been derived from the previously identified Apollo 12 basalt suites (see Previously Identified Apollo 12 Basalt Suites section).

However, care needs to be taken when interpreting petrology and geochemistry from the returned lunar samples as often only small amounts of material are available for analysis, which can result in significant errors and overinterpretation of samples that may be too small to be representative of the parent lava flows from which they originated (e.g., Rhodes et al. 1976; Neal and Taylor 1992; Neal et al. 1994a; Snape et al. 2014). Papike et al. (1976) tried to deal with this problem by averaging published analyses to give a more representative analysis, but acknowledged that replicate analyses were not available for all samples. Sample categorization on the basis of mineral chemistry, rather than bulk chemistry and modal mineralogy, could provide a more accurate way of determining the basalt type and hence the petrogenesis and magmatic evolution of the parent lava. Igneous minerals have distinct major and minor element compositions depending on their origin. The ability to classify small samples using nondestructive methods is important since there are no current plans to return humans to the lunar surface, and gram-sized quantities of material are all that are likely to be returned by future robotic sample missions (e.g., Zolensky et al. 2000; Jolliff et al. 2010; Mitrofanov et al. 2012; Crawford and Joy 2014). Recent work by Fagan et al. (2013) has found that some Apollo mare basalt lava flows can be distinguished based on trace element chemistry in mineral phases, while Zeigler et al. (2012) and Joy (2013) have shown that there are differences in lunar plagioclase in highland rocks enabling classification and grouping of highland rock suites.

PREVIOUSLY IDENTIFIED APOLLO 12 BASALT SUITES

Basalt samples from the Apollo 12 site are mainly low-Ti compositions (bulk rock 1–6 wt% TiO_2 using the classification of Neal and Taylor 1992) with correspondingly high $\delta^{18}O$ (average 5.71 ± 0.11; Hallis et al. 2010) and are commonly grouped into pigeonite, olivine, and ilmenite basalts on the basis of their mineralogy (James and Wright 1972; Rhodes et al. 1977) and bulk rock composition using Mg# (100 × atomic Mg/[Mg + Fe]) and Rb/Sr ratios (Neal et al. 1994a). In order to place our subsequent discussion in context, in this section we briefly summarize what is known about the existing Apollo 12 basalt suites recognized in the literature.

Pigeonite Basalts

The Apollo 12 pigeonite basalts range in texture from porphyritic to coarse microgabbros. They are characterized by highly zoned pyroxene phenocrysts (46–71% modal abundance). Plagioclase (17–48% by mode) has $An_{96–87}$ compositions (Papike et al. 1998). Small amounts (<4%) of olivine may be present. Opaque minerals (3–12% of the mode; Papike et al. 1998) are usually ilmenite, although spinel, Fe-Ni metal, and sulfides may be present. Chemically, these basalts have bulk Mg# <46 and Rb/Sr ratios >0.008 (Neal et al. 1994a, 1994b). Both the pigeonite and olivine basalts are thought to have originated from a relatively shallow source region (100–200 km deep; Longhi 1992; Snyder et al. 1997) containing olivine, orthopyroxene, pigeonite, and augite (Hallis et al. 2014) with subsequent crustal assimilation (up to 3% anorthositic crustal material; Neal et al. 1994b) accounting for the differences between them (Snyder et al. 1997).

Olivine Basalts

The olivine basalts have an average modal mineralogy of 53% pyroxene and are enriched in olivine (20%). They contain an average 19% plagioclase and 7% opaques (Papike et al. 1976). They have Mg# >46 and Rb/Sr >0.008 (Neal et al. 1994a, 1994b). A positive correlation of grain size with normative olivine content is interpreted to result from the settling of olivine (Walker et al. 1976a, 1976b), indicating that many olivine basalts are cumulates.

Ilmenite Basalts

The ilmenite basalts exhibit high modal abundances of ilmenite (8–11%, with an average of 9%). Olivine contents vary (average modal abundance 3.5%). Pyroxene has an average modal content of 59%, and plagioclase 25% (Papike et al. 1998). Ilmenite basalts contain slightly higher REE abundances than the pigeonite and olivine basalts (Hallis et al. 2014). Rb/Sr ratios are <0.008, but bulk Mg# covers the range of the other basalt groups (Neal et al. 1994a, 1994b). Ilmenite basalts are considered to originate from a mantle source region 350–400 km deep (Snyder et al. 1997), similar to the source regions for high-Ti picritic volcanic glass beads (Longhi 1992; Snyder et al. 1997). They result from partial melting of a source which must contain plagioclase in addition to olivine, pigeonite, and orthopyroxene in order to account for Eu anomalies in this basalt group (Hallis et al. 2014).

Feldspathic Basalts

A separate group of feldspathic basalts enriched in aluminium and containing high modal abundances of plagioclase (>38.5% by mode) and a unique isotopic signature has also been proposed (Nyquist et al. 1979, 1981). Despite several samples initially being assigned to this group, the sample 12038 is the sole remaining member of the feldspathic basalt suite (Beaty et al. 1979; Nyquist et al. 1979, 1981; Neal et al. 1994a). This has led to the suggestion that 12038 may have been introduced to the area by impact mixing processes (Neal et al. 1994a) rather than representing a local lava flow. However, Korotev et al. (2011) found two fragments with compositions similar to feldspathic basalts in Apollo 12 soil samples, and the work by Snape et al. (2014) and Alexander et al. (2014) indicated that there may be further feldspathic basalt fragments in the Apollo 12 soil samples. If this is the case, then it is less likely that the feldspathic basalt material was introduced by impacts, and it may, therefore, represent a local lava flow.

Local Lava Flow Stratigraphy

The Apollo 12 basalts are dated as Eratosthenian between 3.1 and 3.3 Ga (Papanastassiou and Wasserburg 1971; Nyquist et al. 1977, 1979). Rhodes et al. (1977) found that the majority of ilmenite basalts were collected in the vicinity of Surveyor crater, and are the only type found in small craters, while most olivine basalts were collected close to Middle Crescent crater (see Supplementary Note 1 in supporting information). Pigeonite basalts were found at locations across the site. From this information, a stratigraphy for the site was constructed (Rhodes et al. 1977). Olivine basalts are believed to have been excavated from the greatest depths and are overlain by ilmenite basalts, with pigeonite basalts possibly occurring between them (Rhodes et al. 1977). If the feldspathic basalts do in fact represent an older flow at the Apollo 12 site (Snyder et al. 1997), then they probably occur beneath the other units and the small number of samples may indicate a lack of craters large enough to excavate material from this flow (Snape et al. 2013, 2014). In addition to the lavas, Korotev et al. (2011) found that the Apollo 12 soils consist of approximately one-third nonmare materials. The nearest exposures of nonmare materials (KREEP-bearing material and impact ejecta) are tens of km away and studies by Korotev et al. (2000, 2011) suggest that the material has been transported to the site by multiple impacts (Jolliff et al. 2000; Korotev et al. 2000; Stöffler et al. 2006).

ANALYTICAL METHODS

The samples studied were provided on loan from the curatorial facility at the Johnson Space Center (JSC). Ten grains from 12070,889 were originally selected for analysis, but 12 were received, indicating that one or two had broken in transit from the US to the UK. Subsequently one of the smaller samples (12070,889_5A) was destroyed during the polishing process. Therefore, results in respect to 11 grains from 12070,889, 1 from 12070,891, and 1 from 12030,187 are given here. Three well-characterized samples (12022,304, 12038,263, and 12063,330) were provided for comparison.

All samples were weighed and assigned individual sample numbers (12070,889_1 to _12, 12070,891_1, and 12030,187_1). They were then split into two or more fragments using a scalpel. The larger splits (labeled 12070,889_1A, etc.) were used for petrological and chemical analysis, while the smaller splits (12070,889_1B, etc.) were kept unmounted for future radiometric dating. The A splits were mounted in EPOTEK epoxy resin blocks and polished with alcohol-based lubricant and diamond paste in order to prevent contamination by water. Samples were carbon coated for electron microprobe analysis.

Energy dispersive spectroscopy (EDS) analyses were obtained using a JEOL JXA-8100 electron microprobe at UCL/Birkbeck with an Oxford Instruments EDS system, operating at 15 keV accelerating voltage with a current of 10 nA to produce backscattered electron (BSE) images and elemental X-ray maps using INCA software. For samples 12030,187 and 12070,891 only, element maps were obtained with a Cameca SX100

electron microprobe at the Natural History Museum, London. Element maps were combined using the GNU Image Manipulation Program (GIMP) following the method used by Joy et al. (2006, 2008, 2010) and Snape et al. (2014). Modal mineralogies were calculated from BSE images and elemental X-ray maps using Adobe Photoshop to identify the phases based on differences in tone. This method has been tested on previously studied Apollo samples and found to be in good agreement with published values (Snape et al. 2011a, 2011b).

Major and minor element mineral analyses were obtained at UCL/Birkbeck using the JEOL JXA 8100 electron microprobe wavelength dispersive system (WDS) with an accelerating voltage of 15 keV, a current of 25 nA, and a beam diameter of 1 μm. Peak counting times were 20 s with a background measurement time of 10 s for all elements except Na, for which counting times were 10 s on peak and 5 s for the background. Analyses were calibrated against standards of natural silicates, oxides, and Specpure® metals, and data were corrected using a ZAF program. Additional corrections were applied for Fe/Co and Ti/V peak overlaps. Errors were calculated using the relative error obtained from repeated measurements of BCR-2 USGS basaltic glass (USGS, 2009). They are generally in the range ±5% with the exception of P_2O_5 where the errors were in the order of ±20%. For oxides present only in trace amounts (<1 wt%) in the BCR-2 (i.e., P_2O_5, Cr_2O_3, V_2O_3, CoO, and NiO), errors were calculated based on the variation in multiple measurements from a homogeneous terrestrial Cr-spinel.

Bulk compositions were calculated by performing multiple EDS raster beam analyses (RBA) across the samples for 480 s count time at 15 keV using the method described by Joy et al. (2010), Snape et al. (2011a, 2011b, 2014) and Alexander et al. (2014). Errors quoted for the bulk compositions are 1σ standard deviations of the five individual RBA. Corrections to account for the difference in host phase densities were applied in accordance with the method of Warren (1997). This method has been previously tested on known lunar samples (Snape et al. 2011b) and found to be comparable with previously published bulk compositions (Compston et al. 1971; Kushiro and Haramura 1971; Wakita and Schmitt 1971; Willis et al. 1971), despite those being obtained on larger mass samples.

Trace element analyses in the major silicate phases, pyroxene, olivine, and plagioclase, were obtained in five analysis sessions using laser ablation inductively coupled plasma–mass spectrometry (LA-ICP-MS) at UCL/Birkbeck. The instrument used was an Agilent 7700X series ICP-MS coupled to an ESI NWR193 (wavelength 193 nm) laser. The pulse frequency was 10 Hz. Data were collected for 60 s, during which time the abundances of 34 elements were monitored (see supporting information). Background conditions were monitored by analyzing He and Ar gas with the laser switched off for 30 s and the sample was then ablated for 30 s with a laser spot size of 25 μm.

LA-ICP-MS data were reduced using the GEMOC Glitter software program (http://www.glitter-gemoc.com/). Ca was used as the internal standard for pyroxene and plagioclase by comparing CaO wt% in minerals previously determined by WDS EMPA and manganese (MnO) was used as the internal standard for olivine. Analyses of pyroxene and plagioclase were externally calibrated with NIST 612-doped synthetic glass, and analyses of olivine were externally calibrated with NIST 610-doped synthetic glass (Pearce et al. 1997). The NIST 610 was monitored as an unknown for pyroxene and plagioclase and NIST 612 was monitored as an unknown for olivine. Repeatability of the NIST 612 standard measurements over all measurement sessions had a total relative standard error range of 0.02–0.10% for all elements analyzed. Accuracy of the NIST 612 standard measurements to NIST 612 published values (Pearce et al. 1997) had a relative difference range of between −7.71% and +7.02% for all elements analyzed and was typically <±1.66%. Repeatability of the NIST 610 standard measurements over all measurement sessions had a total relative standard deviation range of between 0.01 and 0.05% for all elements analyzed and was typically <0.02%. Accuracy of the NIST 610 standard measurements to published values (Pearce et al. 1997) had a relative difference range of −4.41%–+10.78% for all elements analyzed but was typically <±1.8%.

RESULTS

Petrography

Individual fines show a wide variety of textures (Fig. 1), with 8 of the 13 samples (12070,889_3A, 4A, 6A 7A, 9A, 10A, 11A, and 12A) being coarse-grained (up to 0.8 mm). Modal mineralogies are given for all the studied samples in Table 1. Modal percentages given in this section are the percentage of the total analyzed area. These are correct in accordance with the method described in the Previously Identified Apollo 12 Basalt Suites section but, in the case of these eight samples, the modal percentages cannot be used to draw effective comparisons or conclusions because of the small sample size.

The finest-grained samples are 12030,187 and 12070,891. They are porphyritic with phenocrysts of olivine enclosing or partially enclosing spinel and

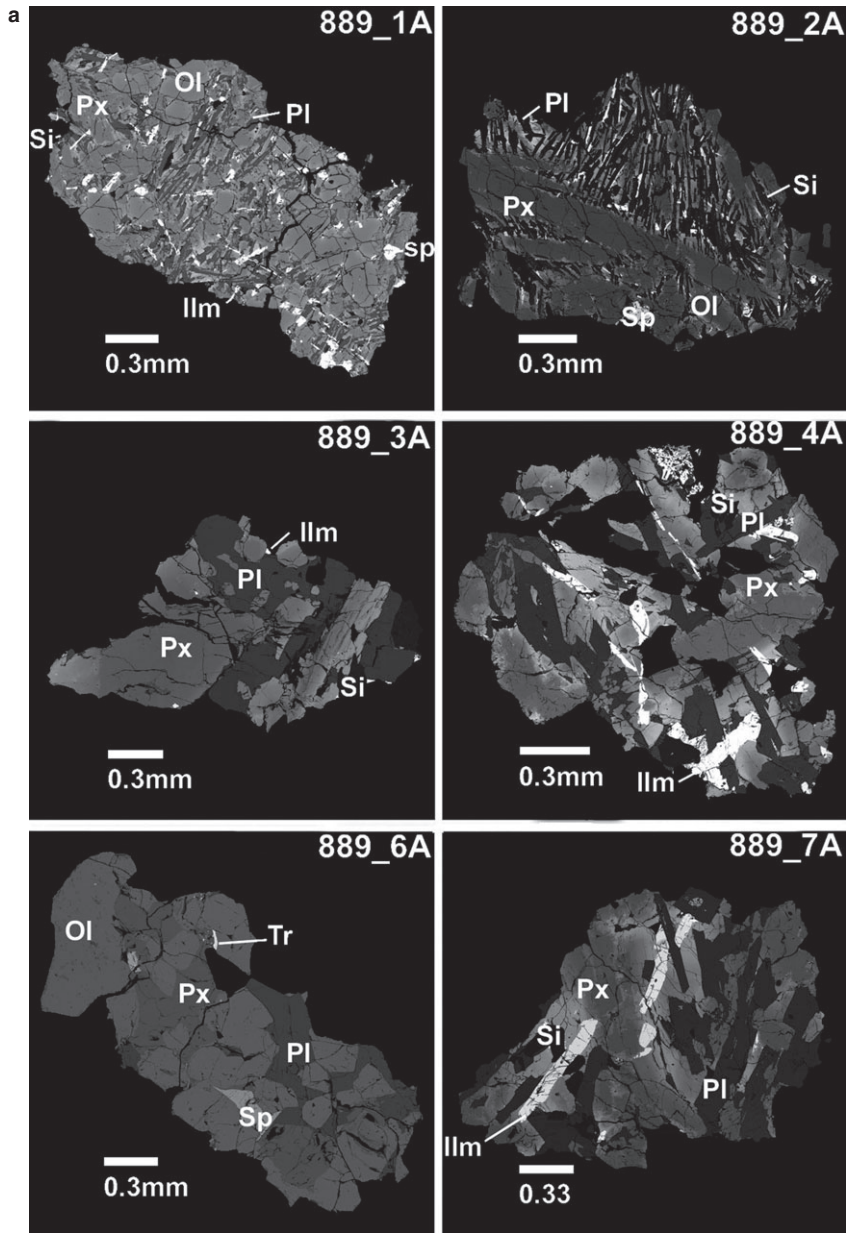

Fig. 1. Backscattered electron (BSE) images samples 12030,187, 12070,891, and 12070, 889_1A to 12A. Abbreviations on BSE images correspond to the following: pyroxene (Px), olivine (Ol), plagioclase (Pl), ilmenite (Ilm), silica (Si), spinel (Sp), and troilite (Tr).

pyroxene, set in a fine-grained microcrystalline to vitrophyric groundmass containing ilmenite, plagioclase, and minor silica (Fig. 1, Table 1). Pyroxene phenocrysts in sample 12070,891 are strongly zoned with a sharp boundary between the different pyroxene compositions and exhibit a soda-straw texture (approximately 0.1 mm where equant, or elongate up to 0.3 mm, Fig. 1b). Some minor constituents may be absent or too small to accurately identify (e.g., sulfides), so it may be that these samples are not truly representative in terms of minor constituents. However, the vitrophyric nature of the groundmass indicates that these samples are more likely to be representative of their parent rocks in terms of their bulk compositions.

Fines from 12070,889 are varied in texture. Porphyritic examples are samples 889_1A (2 × 1 mm, Fig. 1), 889_2A (1.9 × 1.4 mm, Fig. 1), and 889_8A (1.8 × 1.3 mm, Fig. 1). These contain pyroxene and

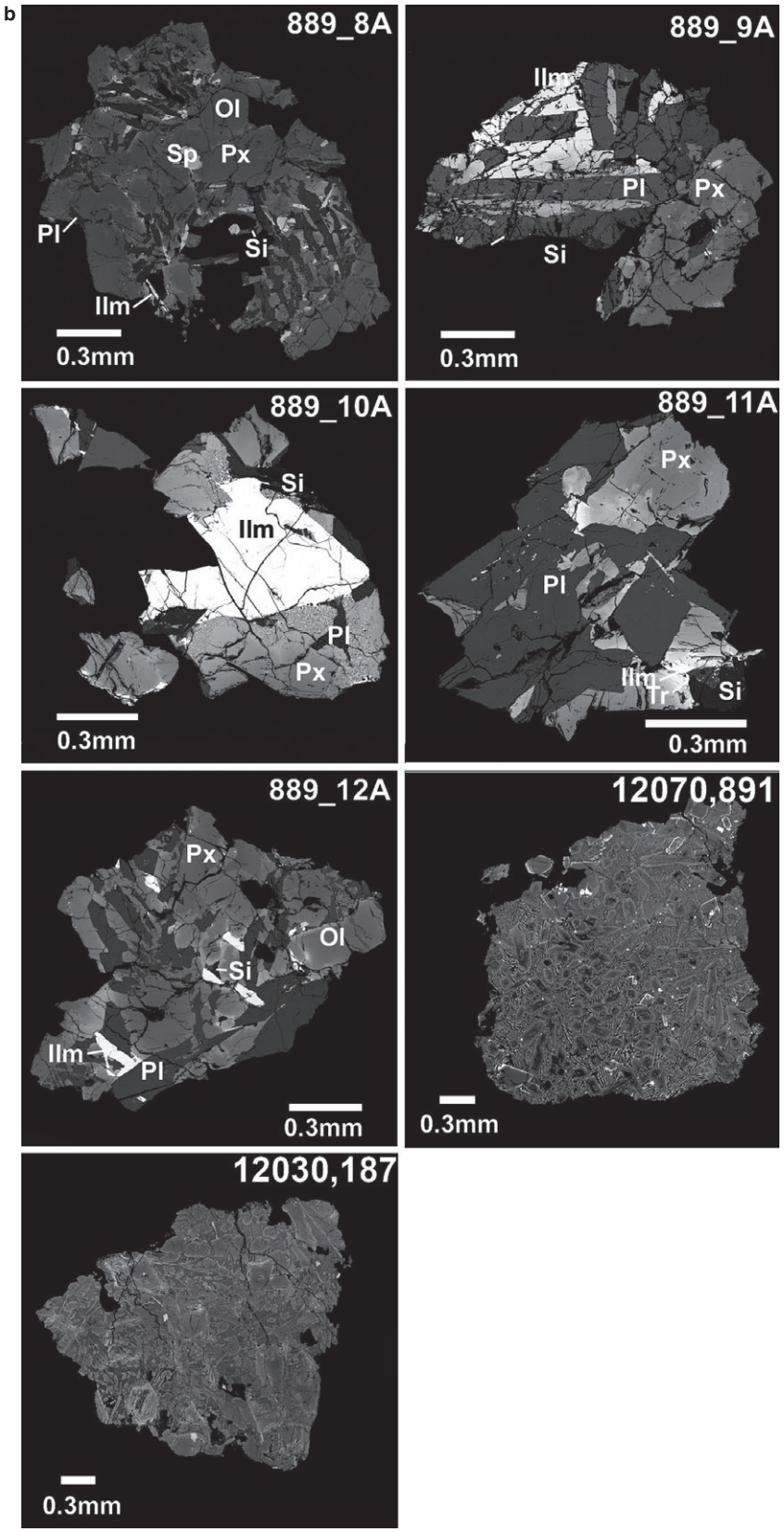

Fig. 1. *Continued*. Backscattered electron (BSE) images samples 12030,187, 12070,891, and 12070, 889_1A to 12A. Abbreviations on BSE images correspond to the following: pyroxene (Px), olivine (Ol), plagioclase (Pl), ilmenite (Ilm), silica (Si), spinel (Sp), and troilite (Tr).

Table 1. Normalized modal mineralogies of basalt fines from lunar soil sample 12070,889. Modal mineralogies are calculated from BSE images and elemental maps using the pixel counting method detailed in the Previously Identified Apollo 12 Basalt Suites section. Based on multiple pixel counts of the same sample, absolute uncertainties on these modal abundances are typically in the range 0–5%.

Modal Mineralogy Calculations (%) 12070,889 (1A to 12A), 12030,187 and 12070,891													
Mineral/Element type	889_1A	889_2A	889_3A	889_4A	889_6A	889_7A	889_8A	889_9A	889_10A	889_11A	889_12A	12030,187	12070,891
Ilmenite	3.6	2.1	0.3	10.4	1.6	4.4	2.9	2.8	36.4	0.5	3.4	5.7	2.1
Chromite/Ulvospinel	1.4	0.7	Trace		0.3	0.1	1.1				Trace	0.2	0.8
Olivine	16.0	3.1		0.1	62.2		9.7				9.1	14.2	3.4
Pyroxene	54.3	61.5	61.7	58.2	21.6	58.9	54.6	55.2	40.4	37.6	50.1	54.8	71.9
Feldspar	23.6	31.8	34.2	29.5	14.2	32.0	31.4	41.5	16.0	57.7	36.1	25.2	21.8
Silica	1.2	0.8	3.8	1.8	4.6	0.3	0.5	7.2	4.2	1.2			
Sulfide				0.1				Trace	0.1				
Total	100.0	100.0	100.0	100.0	100.0	100.0	100.0	100.0	100.0	100.0	100.0	100.0	100.0

Table 2. Bulk chemical compositions in wt% oxide for samples 12070,889_1A to 12A, excluding 5A which was polished away during processing. Mg# = atomic Mg/(Mg + Fe) ×100. Errors for major element oxides are 1σ standard deviation calculated from the repeat raster beam analyses. Propagation of errors is used to calculate the error for Mg#.

Sample	889_1A	889_2A	889_3A	889_4A	889_6A	889_7A	889_8A
Na_2O	0.45 ± 0.04	0.42 ± 0.02	0.49 ± 0.02	0.49 ± 0.04	0.38 ± 0.04	0.42 ± 0.02	0.35 ± 0.03
MgO	6.00 ± 0.13	9.85 ± 0.09	9.31 ± 0.08	5.95 ± 0.04	22.73 ± 0.14	12.85 ± 0.06	13.59 ± 0.09
Al_2O_3	12.28 ± 0.22	10.59 ± 0.09	12.56 ± 0.17	9.65 ± 0.09	5.09 ± 0.16	8.50 ± 0.07	8.87 ± 0.06
SiO_2	45.51 ± 0.11	46.47 ± 0.08	50.08 ± 0.20	42.79 ± 0.08	38.70 ± 0.11	40.84 ± 0.07	44.69 ± 0.07
K_2O	0.10 ± 0.01	0.10 ± 0.02	0.07 ± 0.01	0.20 ± 0.02	0.04 ± 0.01	0.10 ± 0.01	0.08 ± 0.01
CaO	11.78 ± 0.05	10.35 ± 0.04	11.49 ± 0.05	10.27 ± 0.04	4.00 ± 0.08	8.33 ± 0.06	8.76 ± 0.06
TiO_2	5.08 ± 0.07	3.13 ± 0.06	0.89 ± 0.03	5.92 ± 0.06	1.97 ± 0.04	4.54 ± 0.04	2.86 ± 0.04
FeO	18.80 ± 0.20	19.09 ± 0.09	15.11 ± 0.08	24.74 ± 0.11	27.10 ± 0.16	24.42 ± 0.08	20.80 ± 0.10
Total	100.00	100.00	100.00	100.00	100.00	100.00	100.00
Mg#	36.27 ± 1.04	47.90 ± 0.68	52.34 ± 0.29	30.03 ± 0.27	59.92 ± 0.26	48.40 ± 0.28	53.79 ± 0.42
Sample	889_9A	889_10A	889_11A	889_12A	12030_187A	12070_891A	
Na_2O	0.5 ± 0.03	0.08 ± 0.02	0.58 ± 0.02	0.46 ± 0.04	0.30 ± 0.02	0.35 ± 0.02	
MgO	7.39 ± 0.06	2.55 ± 0.07	5.43 ± 0.07	10.04 ± 0.14	11.87 ± 0.08	8.16 ± 0.04	
Al_2O_3	15.64 ± 0.14	1.68 ± 0.05	19.75 ± 0.11	11.94 ± 0.19	8.13 ± 0.05	9.93 ± 0.04	
SiO_2	46.39 ± 0.24	21.47 ± 0.26	46.53 ± 0.07	43.64 ± 0.06	44.71 ± 0.06	46.29 ± 0.06	
K_2O	0.12 ± 0.01	0.09 ± 0.02	0.09 ± 0.01	0.10 ± 0.01	0.07 ± 0.01	0.09 ± 0.02	
CaO	11.63 ± 0.09	4.76 ± 0.07	14.42 ± 0.08	11.00 ± 0.08	8.52 ± 0.04	10.26 ± 0.05	
TiO_2	2.62 ± 0.19	28.64 ± 0.31	1.13 ± 0.03	3.92 ± 0.03	3.38 ± 0.03	3.79 ± 0.02	
FeO	15.69 ± 0.22	40.73 ± 0.11	12.05 ± 0.10	18.90 ± 0.04	22.44 ± 0.08	20.32 ± 0.06	
Total	100.00	100.00	100.00	100.00	99.42	99.18	
Mg#	45.65 ± 0.50	10.04 ± 0.29	44.55 ± 0.70	48.64 ± 0.85	48.53 ± 0.16	42.73 ± 0.12	

olivine phenocrysts (glomerophyric in 889_1A) set in a groundmass of pyroxene, plagioclase, ilmenite, and minor silica.

Coarse-grained samples are also present in this batch. Samples 889_4A (1.8 × 1.6 mm, Fig. 1), 889_7A (1.4 × 1.5 mm, Fig. 1), and 889_12A (1.1 × 1.7 mm) are subophitic with large-zoned pyroxene crystals (50–59% by mode), blocky to anhedral plagioclase (30–36%) and coarse laths of ilmenite (3–10%). Sample 889_12A also contains rounded olivine crystals (9%) and silica (1%). Sample 889_4A contains late-stage patches of Fe-rich mesostasis with a swiss-cheese texture resulting from the breakdown of pyroxferroite. The mesostasis contains silica and fayalite, together with pyroxene and ilmenite. Small patches of mesostasis are also found in 889_7A.

Sample 889_6A (2.2 × 1 mm, Fig. 1) has a granular texture with a high modal abundance of olivine (62%). This abundance of coarse olivine crystals and less abundant pyroxene and interstitial plagioclase may indicate that this is a cumulate sample. Pyroxene (22%) is less zoned than other samples and does not exhibit Fe enrichment at the rims. Minor ilmenite (2%), Cr-spinel, and sulfides are also present (<1%).

Particularly coarse-grained samples have grain sizes of a similar scale to the overall size of the sample (>0.6 mm) and cannot therefore be representative of their parent melts. They include sample 889_3A (1.7 × 1.1 mm, Fig. 1) which has a grain size up to 0.9 mm, consisting of zoned subhedral pyroxene crystals (62%) partially enclosed by anhedral masses of plagioclase (34%). Minor ilmenite (<1%), Cr-spinel crystals, and patches of interstitial silica (4%) are also present. Sample 889_9A (1.1 × 1.5 mm, Fig. 1) consists of pyroxene (55%), feldspar (42%), ilmenite (3%), and minor silica (<1%).

Sample 889_10A (1 × 0.8 mm) is largely formed of a single ilmenite grain (0.5 × 0.8 mm) surrounded by patches of symplectite (Fig. 1, Table 1). Fe-rich pyroxene/pyroxferroite is present in the symplectite regions together with a K-rich glass phase whose proximity to the fayalite indicates that it formed as part of this late-stage assemblage. Other minerals include pyroxene (40%), plagioclase (16%), silica (7%), and a single sulfide crystal, together with occasional small (approximately 10 μm) apatites. Sample 889_11A (0.8 × 0.9 mm, Fig. 1) is dominated by coarse, blocky plagioclase (58%) with zoned pyroxene (38%), patches of silica (4%), and one small (100 × 50 μm) symplectite area in a region containing Fe-rich pyroxene, a small fragment of ilmenite and minor sulfide.

Bulk Compositions

Bulk compositions are given in Table 2. All samples have low-Ti bulk compositions in accordance with the

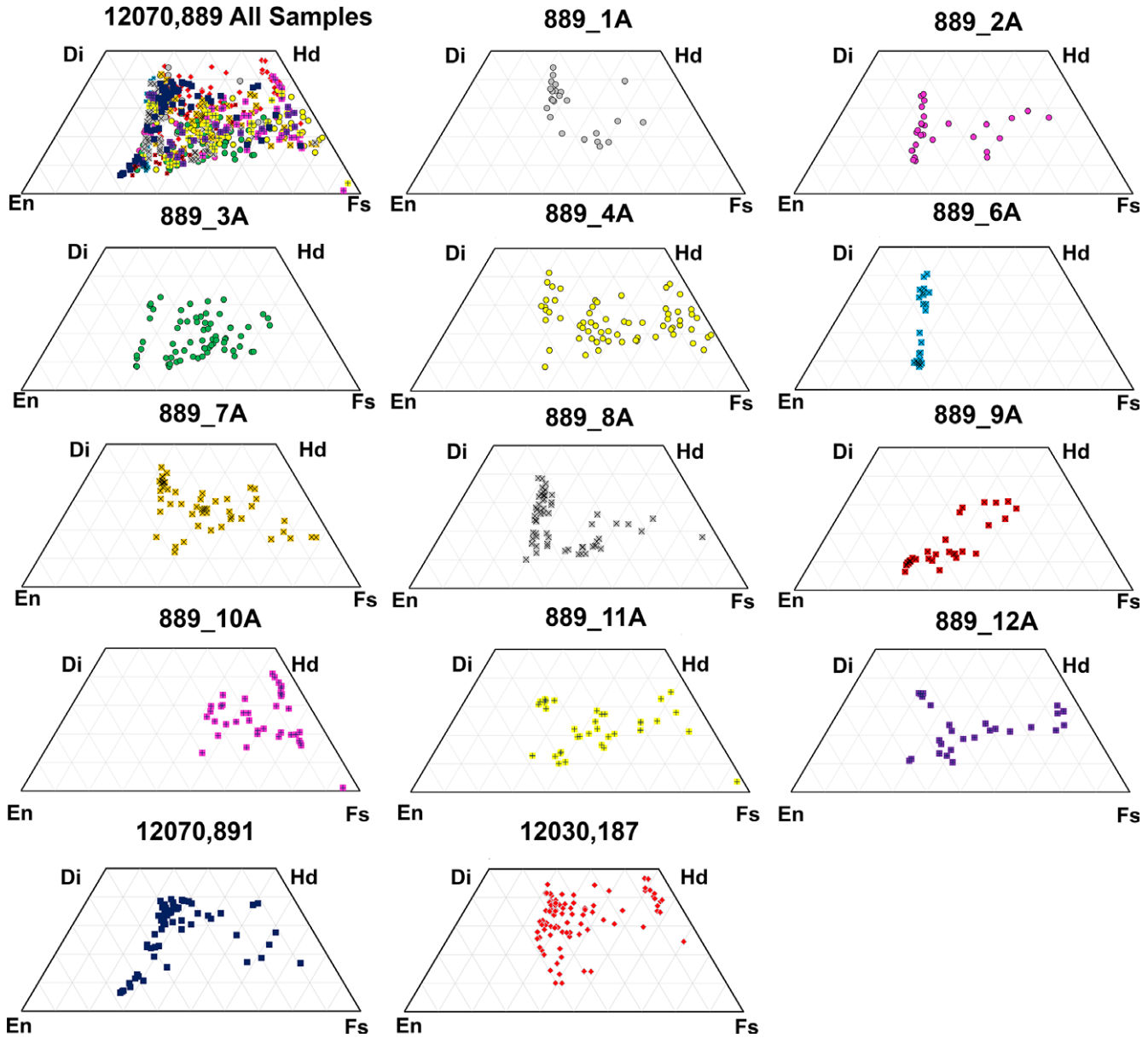

Fig. 2. Pyroxene quadrilateral plots showing pyroxene compositions in previously published Apollo 12 basalt groups, with trends indicated from Papike et al. (1976), together with pyroxene compositions from lunar soil sample 12070,889, and lunar samples 12030,187 and 12070,891. Di = diopside, En = enstatite, Hd = hedenbergite, and Fs = ferrosilite. Dashed line indicated in 12070,891 indicates the compositional gap discussed in the text. Pigeonite compositions have Wo <20.

classification of Neal and Taylor (1992) with 1–6 wt% TiO_2 contents, except for 889_10A which is dominated by a large ilmenite crystal and is, therefore, probably unrepresentative of its parent basalt. Eight of the samples in this set have grain sizes >0.6 mm and are probably unrepresentative of their parent basalts. Al_2O_3 contents for 889_11A are particularly high (19.8 wt%) because the sample is dominated by plagioclase. Sample 889_6A has low Al and Ca contents (5.1 wt% Al_2O_3 and 4 wt% CaO, respectively) and the highest Mg# (60) of all the samples. It also has lower SiO_2 content (38.7 wt%), likely resulting from the large modal abundance of olivine and the cumulate nature of this sample. With the exception of the unrepresentative sample 889_10A, most samples have a narrow range of SiO_2 content (40.8–50.1 wt%).

Mineral Chemistry

Pyroxene

Pyroxene crystals ($En_{1–64}$ $Fs_{20–94}$ $Wo_{6–44}$, Figs. 2–4) generally show the typical range of compositions

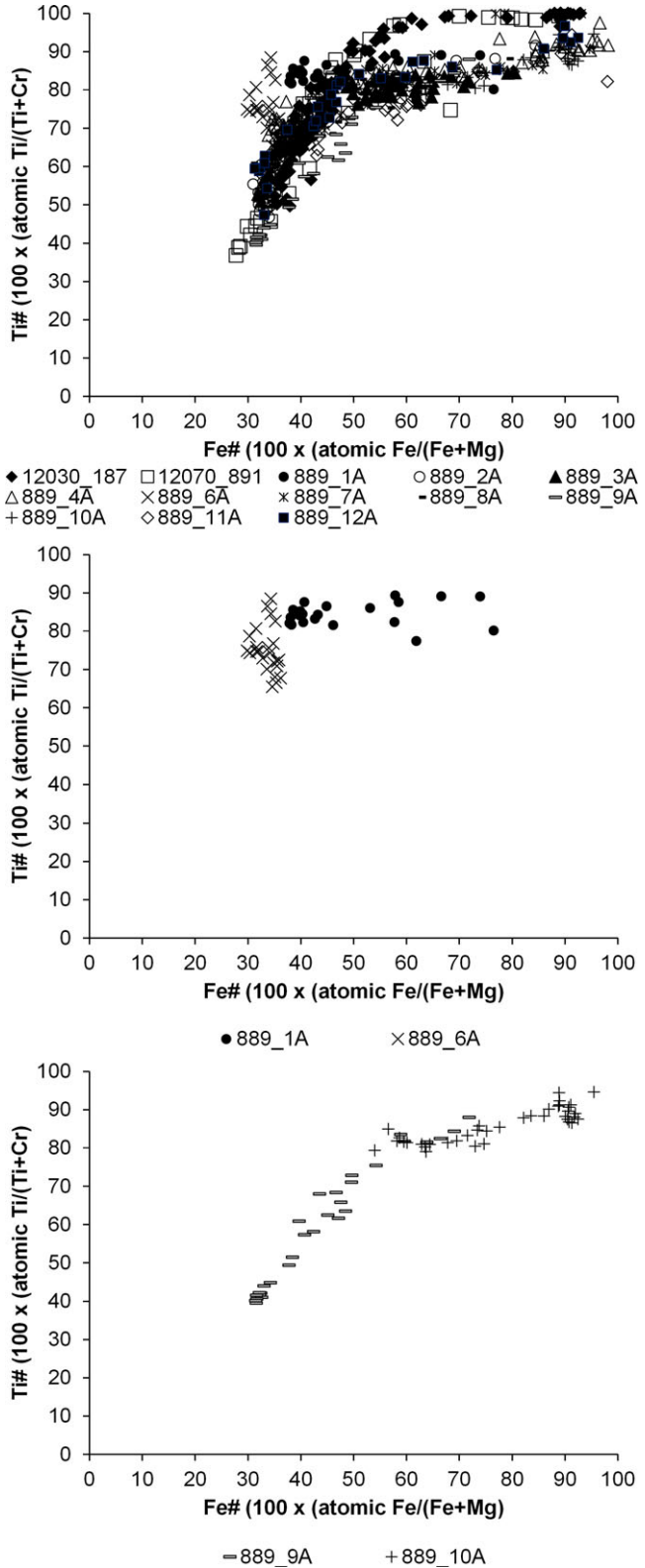

Fig. 3. Fe# (100 × atomic Fe/[Fe+Mg]) versus Ti# (100 × atomic Ti/[Ti+Cr]) for pyroxene phases in 12070,889, 12070,891, and 12030,187 showing crystallization trends.

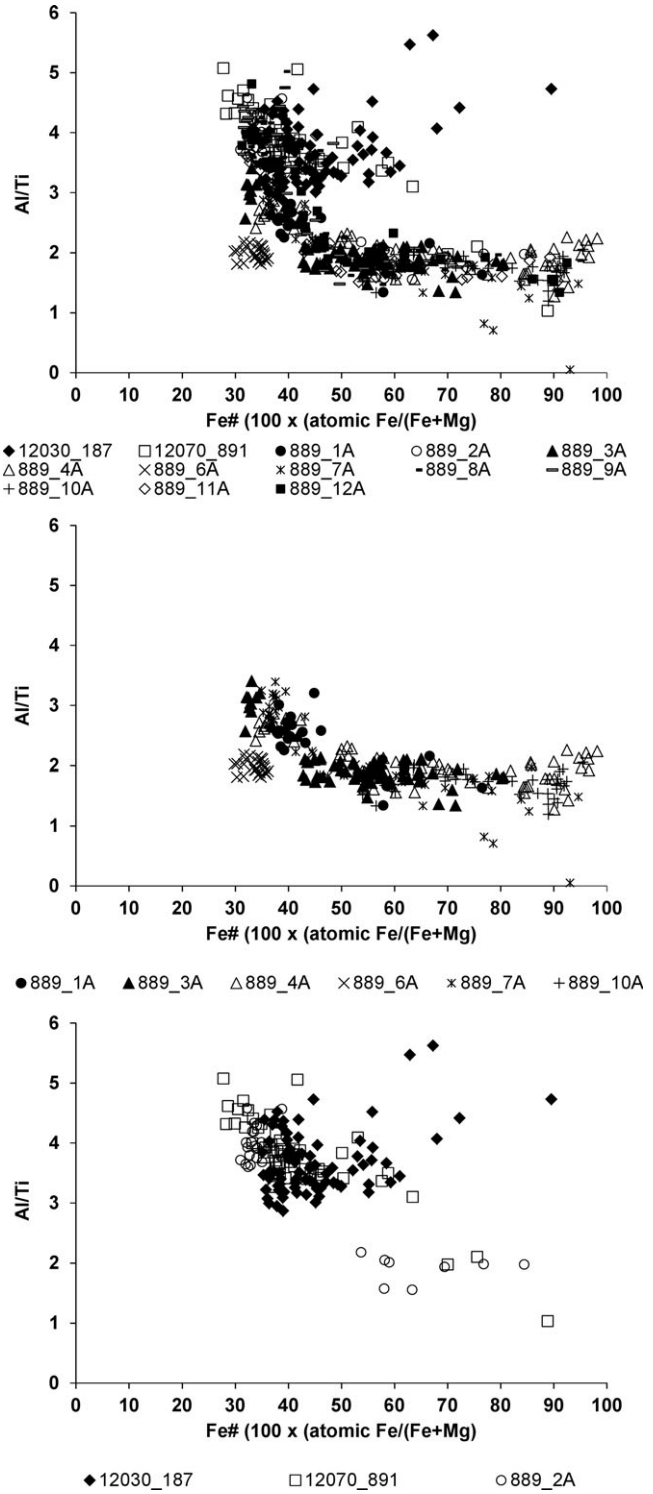

Fig. 4. Fe# (100 × atomic Fe/[Fe+Mg]) versus Atomic Al/Ti for pyroxene phases in 12070,889, 12070,891, and 12030,187 showing crystallization trends.

expected from Apollo 12 samples (Papike et al. 1976). Zoning from core to rim is seen in most samples with either pigeonite or augite cores mantled by augite. More Fe-rich compositions are seen toward the rims of the crystals with extreme Fe-enrichment in some samples (e.g., 889_4A, 10A, and 11A) as expected from a fractionating melt which became more Fe rich over time. Late-stage groundmass pyroxene crystals are also more Fe rich as expected.

Sample 889_6A is equilibrated and its pyroxenes show the least zoning in these samples ($En_{41–60}Fs_{18–33}Wo_{8–41}$). Pyroxene mainly occurs as separate pigeonite and augite crystals, although occasionally pyroxene is zoned from augite cores to pigeonite rims. In addition all pyroxenes are Mg rich (Mg# 63.8–70.1) and little Fe enrichment is seen in the rims.

Sample 889_10A contains zoned pyroxenes which are all Fe rich, with extreme enrichment in the rims {$En_{4–40}Fs_{41–94}Wo_{1–33}$, Fe# (100 × atomic Fe/[Mg + Fe]) 58–96}, although this may be an effect of sampling bias, as pyroxene crystals are close to the Fe-rich symplectites. Pyroxene is mostly augite, occasionally rimmed with pigeonite, and one separate pigeonite crystal was analyzed. Pyroxene compositions within the symplectite areas are $En_{5–7}Fs_{54–67}Wo_{29–41}$.

Pyroxene crystals in 12030,187 exhibit high-Wo content in the rims of some larger (up to 0.6 mm diameter; Fig. 1) crystals and also in the groundmass pyroxene. Most pyroxenes are augitic, with rare smaller pigeonite crystals (approximately 0.1 mm diameter) to hedenbergite compositions in the groundmass pyroxenes and occasional pigeonite compositions in the zoned rims of larger augite crystals. Pyroxene crystals in 12070,891 are strongly zoned with more primitive, Mg-rich pigeonite cores (Mg# up to 72) than those in 12030,187, and augite mantles and rims. A discontinuity in the larger pyroxene phenocrysts can be seen in the trend from pigeonite to augite (Fig. 2).

Trace element abundances were measured in pyroxene crystals from all samples (Fig. 5). These showed a range of concentrations, with cores exhibiting lower concentrations than mantles, and rims showing the highest concentrations. Rare earth elements (REE) have chondrite-normalized (subscript "cn"; CI chondrite values from Anders and Grevesse 1989) values that are generally lower in light-REE (LREE) relative to heavy-REE (HREE) with $(La/Lu)_{cn}$ values ranging from 0.02 to 1.96, where analyses were above detection limits. Negative Eu anomalies are present in all pyroxenes, with Eu/Eu* (chondrite-normalized Eu/$\sqrt{[Sm \times Gd]}$) ranging from 0.12 to 0.6, again where measurements were above detection limits.

The REE abundances are low in 889_2A, 3A, 8A, and 9A (Fig. 5a), with only two rim measurements

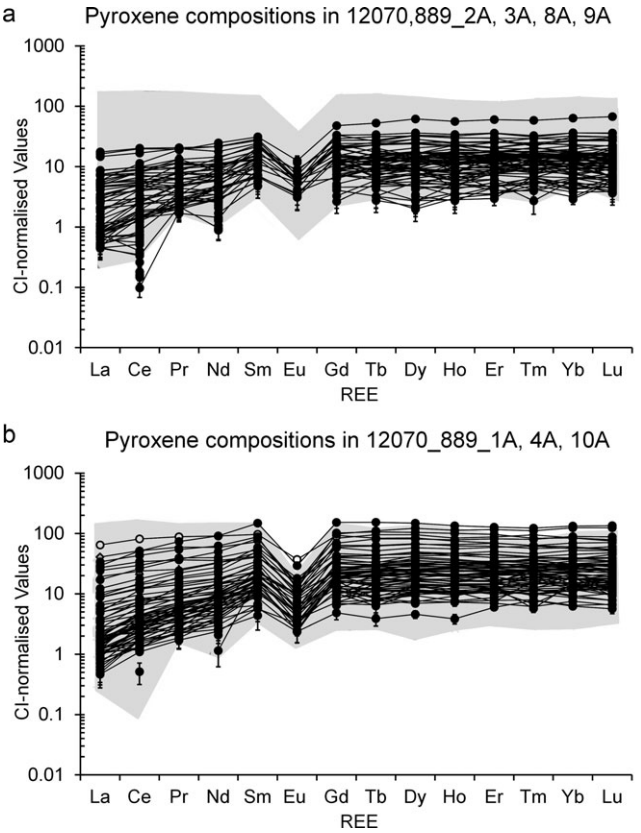

Fig. 5. Chondrite normalized (Anders and Grevesse 1989) REE concentrations in pyroxenes. a) Samples 12070,889_2A, 3A, 8A, and 9A with shaded region representing all other samples from this study. b) Samples 12070,889_1A 4A, and 10A with shaded regions representing the range of other samples from this study. Errors represent 1σ errors as reported by the Glitter software.

having detectable Eu concentrations, and no trace elements were measured in concentrations greater than 30 × CI in 889_2A, 36 × CI in 889_3A, or 33 × CI in 889_8A. High trace element abundances, particularly in the rims, are seen in 889_1A, 4A, and 10A (Fig. 5b), with concentrations up to 96 × CI (Sm) in 889_1A, up to 153 × (Tb and Gd) in 889_4A, and up to 106 × CI in 889_10A (Tb).

Plagioclase Feldspar

Plagioclase is abundant in most samples, and is typically anorthite ($An_{80–93}$, Fig. 6) with only 889_6A and 8A showing lower values ($An_{59–92}$ in 889_6A, and $An_{77–92}$ for 8A). The highest anorthite contents together with the smallest variation are seen in 889_11A ($An_{90–93}$).

Trace element concentrations in plagioclase were measured in the samples where crystal size permitted analysis (>100 μm width; samples 889_3A, 4A, 6A, 7A, 9A, 10A, 11A, and 12A, supporting information). All analyses showed a positive Eu anomaly with Eu

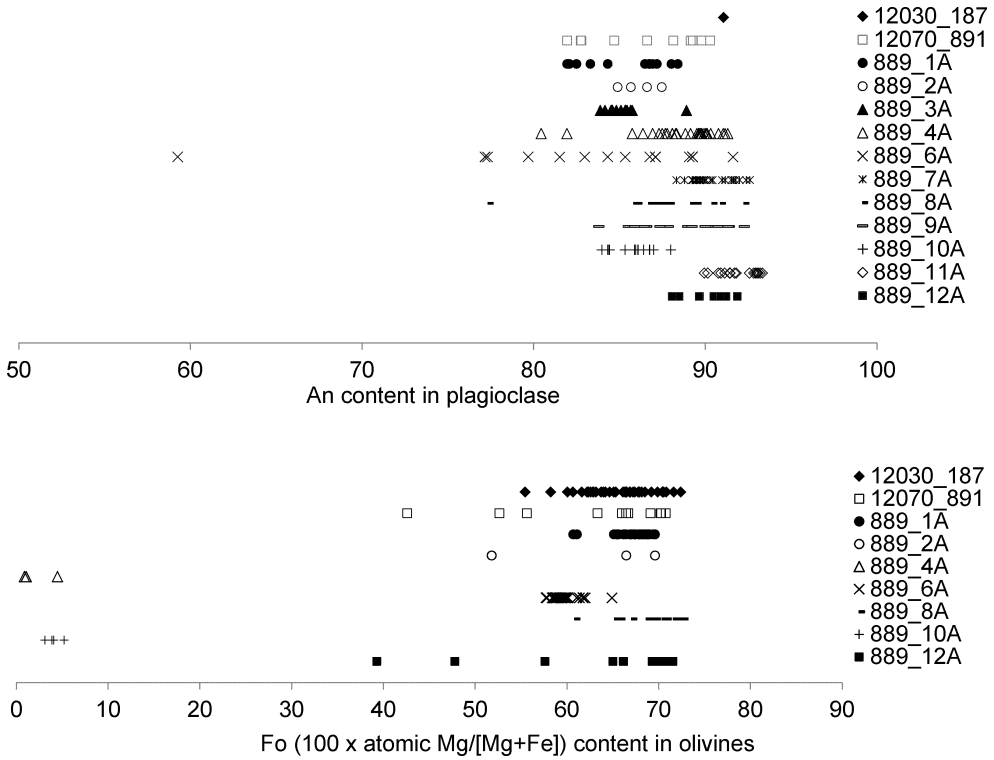

Fig. 6. Compositions of plagioclase and olivine in 12070,889, 12070,891, and 12030,187. a) Anorthite (100 × atomic Ca/[Ca+Na+K]) content of individual plagioclase measurements. b) Fo (100 × atomic Mg/[Mg+Fe]) content in olivine.

concentrations ranging from 1.06 ppm (19 × CI) in 889_9A up to 11.97 ppm (214 × CI) in 889_3A. Sr concentrations were also highest in 889_3A (up to 1324 ppm) and lowest in 889_9A (up to 261 ppm).

Olivine

Olivine Fo (100 × atomic Mg/[Mg+Fe]) content range from 0 to 73 (Fig. 6). Samples 889_4A and 10A contain only fayalitic olivine ($Fo_{0–5}$ in 889_4A and $Fo_{3–5}$ in 889_10A), which is present in the mesostasis of 889_4A and in symplectites in 889_10A. Olivine crystals with the highest magnesium contents are found in 889_8A ($Fo_{61–73}$) and 889_1A ($Fo_{61–70}$). The narrowest range of compositions is seen in sample 889_6A, and olivines in this sample have lower Cr_2O_3 content but a wider range of CaO content than seen in other samples.

Trace element concentrations were measured in olivine (Fig. 7), except for olivine associated with the mesostasis in 889_4A and 10A. Results show significant variations between the samples. Sample 889_2A has higher Co (141–162 ppm) and Ni (246–316 ppm) contents than other samples as well as the highest Mn concentrations (2780–3028 ppm). This sample also has high V content and low Ti content. Sample 12070,889_6A contains olivine crystals which also have not only high Mn (2440–2982 ppm) and Y (1–5 ppm) concentrations but also contains the lowest Ni content (32–64 ppm). Ranges are restricted within the crystals indicating some homogenization.

Chromite, Ulvöspinel, Ilmenite, and Other Phases

Spinel is found in most samples from trace amounts up to 1.4% by mode, although it is not seen in samples 889_4A, 9A, 10A, or 11A. Spinel is commonly associated with or included in olivine, implying that it crystallized early. Crystallization trends of pyroxene in the samples (Figs. 3 and 4) confirm early crystallization. Spinel is often zoned from chromite to ulvöspinel (Samples 889_1A, 2A, and 3A, 12030,187, 12070,891, although 889_3A has more equilibrated compositions). A compositional gap between Cr-rich and Ti-rich spinels (Fig. 8) has been interpreted as partial resorption of chromite as a result of slow cooling (Arai et al. 1996). Sample 889_8A contains chromite only and 889_7A has ulvöspinel only (Fig. 8).

All samples contain ilmenite, which displays variable amounts of MgO (0–5 wt%). The highest MgO content is seen in 889_6A (5.3 wt%), although there is only one coarse ilmenite crystal in this sample. This indicates that the melt from which this sample originated was Mg rich, since ilmenite composition correlates with bulk rock composition and is believed to

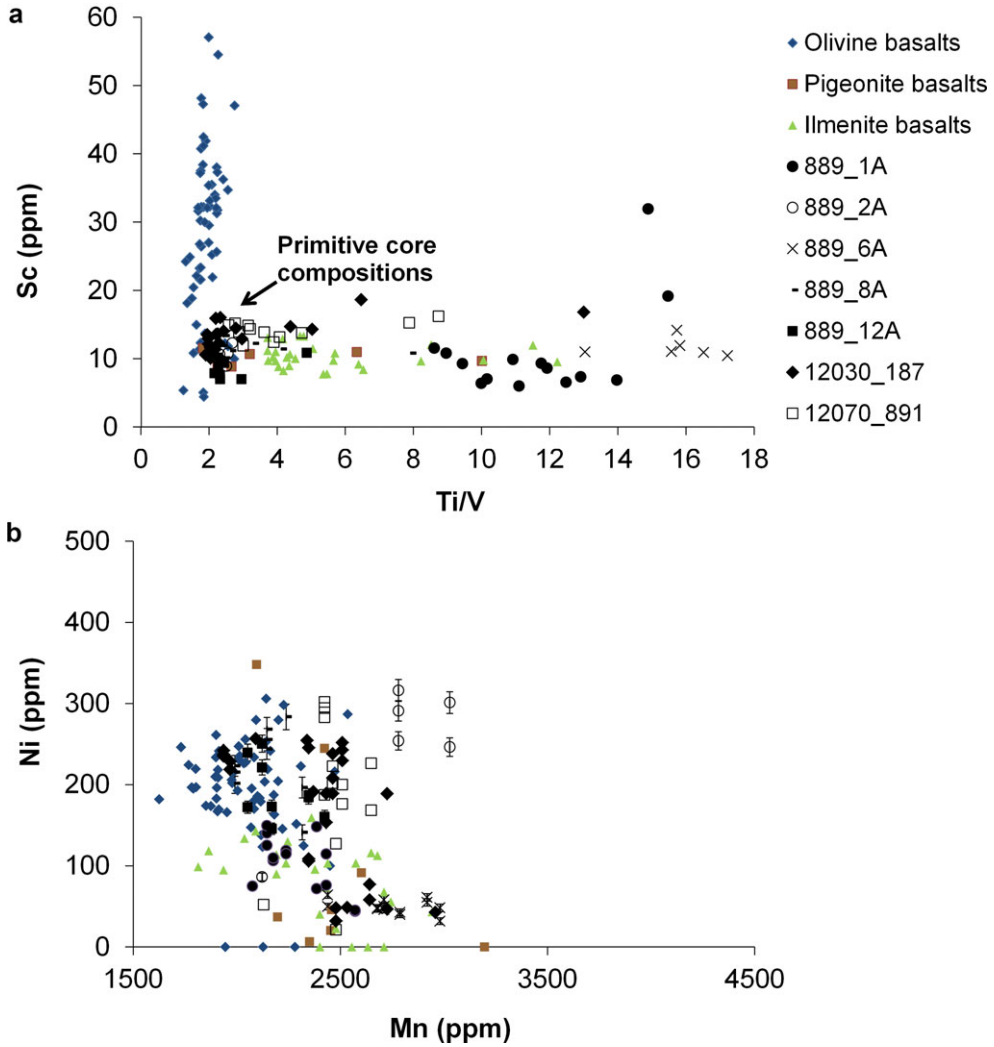

Fig. 7. Trace elements in olivine. a) Sc (ppm) versus Ti/V in olivine crystals in 12070,889 samples and 12070,891 and 12030, 187. Comparative data for Apollo 12 basalt suites are from Fagan et al. (2013). b) Ni (ppm) versus Mn (ppm). Comparative data for (b) from Shearer and Papike (2005), Schnare et al. (2008), and Borg et al. (2009).

reflect magma chemistry rather than pressure (Papike et al. 1998). More variable results are seen in other samples but no measurements >2.6 wt% MgO were found in any other ilmenite crystals. The lowest MgO content is found in ilmenites from 889_9A (<0.10 wt%).

All samples, with the exception of 889_6A, contain silica, and analyses of a late-stage K-rich glass phase were also made in 889_11A (7.9 wt% K_2O). Rare sulfides are present in 889_6A, 10A, and 11A, which were small (approximately 10–20 μm) and gave poor analytical results but appear to be troilite. The sulfide analyzed in 889_10A contained Mo (approximately 0.4 wt%), a further indication of the reduced nature of this sample. Apatite crystals were too small to analyze effectively (<20 μm) in samples 889_4A, 7A, and 10A, where they were also associated with late-stage assemblages.

DISCUSSION

Estimation of Parental Melt Compositions Through Mineral Analysis

The equilibrium parent melt Mg# has been modeled from olivine compositions in the samples and the liquidus olivine Mg# has been predicted from the bulk compositions using the methods and equations described in many previous publications (e.g., Roeder and Emslie 1970; Papike et al. 1976; Dungan and Brown 1977; Joy et al. 2008) and applying a distribution coefficient (K_d) of 0.33, applicable for lunar melts (Grove and Vaniman 1978; Longhi et al. 1978).

This procedure works well for most samples that contain olivine (Table 3) as the bulk rock Mg# and olivine Mg# can be recreated with reasonable accuracy

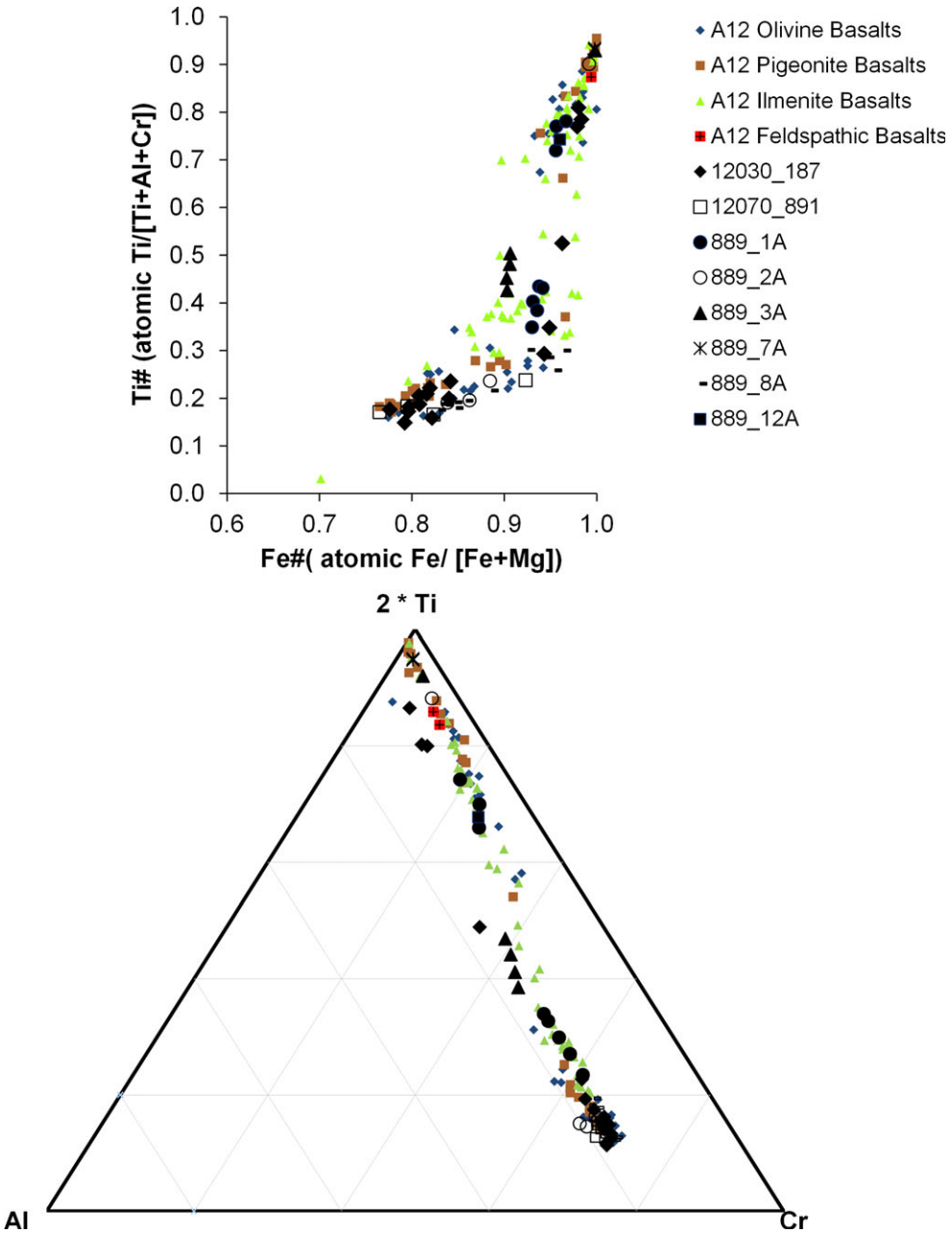

Fig. 8. Spinel compositions and crystallization trends in 12070,889_1A, 2A, 3A, 7A, 8A, and 12A and 12020,891 and 12030,187 showing the Fe# versus Ti# trends and a ternary plot of atomic % 2 × Ti, Cr, Al. Compositions in the plots are compared to other Apollo 12 basalt spinels. Data from Brett et al. (1971); Brown et al. (1971); Cameron (1971); Champness et al. (1971); Dungan and Brown (1977); El Goresy et al. (1971); Gibb et al. (1970); Haggerty and Meyer (1970); Keil et al. (1971); Kushiro and Haramura (1971); Reid (1971); Taylor et al. (1971); and Weill et al. (1971). Spinel compositions mostly show a trend typically seen as a result of mare basalt fractionation in Apollo 12 and Apollo 15 low-Ti basalts (Papike et al. 1991), although compositions for 889_3A are more equilibrated, possibly as a result of slow cooling in a coarser grained sample, as discussed in the text.

(generally within approximately 10% of measured values for 889_1A, 2A, 8A, and 12A, and 12070,891 and 12030,187). Therefore, measured bulk compositions of these samples are likely to be representative of their parent melts in terms of major element constituents. Most of the coarser grained samples do not contain olivine, with the exception of sample 889_6A in which olivine lacks the high Mg# predicted by the bulk rock Mg#. This sample may be a cumulate as suggested by the excess olivine, the compositionally equilibrated

Table 3. Modeled equilibrium parent melt Mg# from olivine compositions and predicted equilibrium Mg# of olivine predicted by bulk rock Mg#. Samples modeled are samples 889_1A, 2A, 6A, 8A, and 12A. Most other samples do not contain olivine and samples 889_4A and 10A contain late-stage fayalite only and are therefore not included.

Sample	Most primitive measured olivine Mg#	Predicted equilibrium melt Mg#	Measured bulk rock Mg#	Predicted equilibrium olivine Mg#
889_1A	68.0	41.2	36.3	63.3
889_2A	69.6	43.1	47.9	73.6
889_6A	64.9	37.9	59.9	81.9
889_8A	72.6	46.7	53.8	77.9
889_12A	71.6	45.4	48.6	74.2
12070,891	70.5	44.1	41.7	68.4
12030,187	72.0	46.1	48.5	74.1

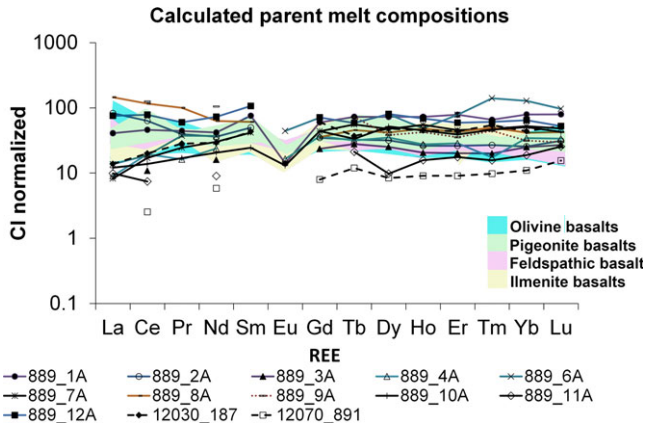

Fig. 9. CI chondrite-normalized (Anders and Grevesse 1989) calculated parent melt REE profiles for samples from 12070,889, 12030,187, and 12070,891 using the method of Sun and Liang (2012, 2013). Shaded regions correspond to data for those groups from the mare basalt database (http://www.nd.edu/~cneal/Lunar-L).

nature of the mineral phases, and the compositional variation in intercumulus plagioclase. Crystal settling may have removed early crystallized phases of olivine and Cr-spinel from a coexisting olivine-rich cumulate (Green et al. 1971; Papike et al. 1998). This would also account for the low Ni content in olivine in this sample as Ni content in olivine in mare basalts decreases with decreasing Mg# (Longhi et al. 2010).

Evaluation of bulk rock TiO_2 content can be made by examining the pyroxene Fe# versus Ti# (atomic Ti/[Ti+Cr] × 100), using the method described by Arai et al. (1996). At pyroxene Fe# 50, the corresponding range of Ti# is between 73 (889_9A) and 90 (12070,891) (Fig. 3). This gives reconstructed bulk TiO_2 values of 2.5–5.0 wt%, indicating that the chips are all low-Ti basalts. Samples whose bulk chemistries do not reflect these values are 889_3A, 6A, 10A, and 11A, which are all samples with grain sizes >0.6 mm.

Pyroxene is present in all samples but, although it is useful to examine crystallization trends (Figs. 3 and 4), none of the major or trace elements or element ratios in pyroxene appear to discriminate between the different basalt types. Pyroxene crystallizes over a large range of pressures and temperatures (Papike et al. 1998; Karner et al. 2006), resulting in wide compositional variations and chemical changes, as well as further subsequent subsolidus equilibration. However, pyroxene can be used to calculate parent melt compositions (e.g., Joy et al. 2008; Schnare et al. 2008; Snape et al. 2014). A common approach (e.g., Jones 1995; Schnare et al. 2008) is to invert the trace element data for primitive core compositions obtained by LA-ICP-MS. There are limited options available when choosing distribution coefficients for this purpose due to the lack of published data across a range of minerals for lunar oxygen fugacity, chemistry, and pressure conditions. We find that lunar mare basalt melt compositions can be most effectively calculated using the mineral-melt calculations of Sun and Liang (2012, 2013), as applied by Snape et al. (2014), in order to calculate kD values for pyroxene phases with different major element compositions. These distribution coefficients have been specifically developed for lunar picritic melts and take into account the composition of the pyroxene phase, so that separate kD values are calculated for REE that vary according to the major element compositions. This method was tested using three well-documented samples, two ilmenite basalts (samples 12022 and 12063) and the feldspathic basalt (sample 12038), and comparing the results with published data of their bulk compositions. The most primitive pyroxene core composition data were used for this test (Mg# 66 for 12063, Mg# 60 for 12022, and Mg# 65 for 12038). The calculated melt compositions are in reasonable agreement with CI-normalized abundances, generally falling between published bulk compositions for these samples (see figure in supporting information). Following this successful test, parent melt compositions were calculated from the most primitive (i.e., highest Mg#) pyroxene core compositions from samples 12070,889, 12070,891, and 12030,187. Results indicate that most samples contain similar REE concentrations to Apollo 12 mare basalts groups (Fig. 9). However, the REE concentrations measured are similar for the different basalt groups and there are significant overlaps, making it impossible to differentiate basalt types from parent melt compositions alone. Sample 889_8A has REE concentrations slightly higher than

other olivine basalts, but this is a relatively coarse-grained sample and results need to be treated with some caution as subsolidus equilibration and elemental diffusion may have affected the core compositions.

Comparison with Basaltic Samples from the Apollo 12 Landing Site

Comparison Using Pyroxene Chemistry

Pyroxene chemistry is useful for inferring trends in different samples by comparing Fe# and Ti# (Fig. 3). Most pyroxenes follow a typical crystallization sequence of Ti# increasing with Fe# as expected from a fractionating melt. Some individual discrepancies are observed, most notably in 889_6A, which contains equilibrated pyroxenes with very little variation in chemistry. Crystallization trends also show where Cr-spinel was a cocrystallizing phase as Ti# increases rapidly in pyroxene during this stage because Cr partitioned into the Cr-spinel (Fig. 3). This trend is apparent in most samples, other than 889_10A, which is a coarse-grained Fe-rich sample with a late-stage mineral assemblage. In addition, samples 889_1A, 889_4A, 7A, and 11A show a less dramatic increase in Ti# with a higher value at the start of the trend. This trend flattens out when ilmenite reaches the liquidus as Ti is partitioned into that phase, which occurs at Fe# approximately 45–55 for most samples. This is not observed in 889_6A, because of the equilibration of pyroxene and a lack of ilmenite in the sample, indicating that ilmenite was a late-stage mineral which had only just reached the liquidus.

The cation ratio of Al/Ti in pyroxene can also be useful for inferring concurrent trends in crystallization (Fig. 4). Most samples fall onto one of two trends. Steep trends are exhibited by 889_2A, 8A, 9A, 11A, and 12A with a sharp decline in Al/Ti while Fe# increases slowly. Cocrystallization of ilmenite at approximately Fe# 50 is confirmed by the flattening of the trend at this point. Shallow trends with less variation in Al/Ti are seen in 889_1A, 3A, 4A, and 7A, which probably indicates more cocrystallization of the phases present, or that they crystallized from a more evolved melt. The flattening at Fe# (approximately 40) indicates ilmenite crystallization was concurrent earlier than in samples with the steeper trend. Again sample 889_6A does not show these trends, and Al/Ti ratios are low and of limited range (1.8–2.2, Fig. 4). This indicates that pyroxene crystallization was complete before the onset of crystallization of ilmenite and plagioclase which formed as late-stage intercumulus phases.

Sample 889_7A exhibits the lowest Al/Ti at high Fe# (0.05 at Fe# 94), indicating a relatively Ti-rich melt. Cocrystallization of ilmenite at Fe# approximately 50 for 889_4A, and Fe# approximately 45 in 889_7A, is indicated by a compositional gap, while plagioclase cocrystallization appears to be fairly concurrent through the sequence, commencing at Fe# approximately 40. Final crystallization of silica, and an Fe-rich mesostasis containing fayalite, ilmenite, and silica, is seen from the textures of these samples.

A roughly linear trend of decreasing Al/Ti with increasing Fe# in sample 12070,891 implies cocrystallization of plagioclase, but the lack of a coherent trend probably results from rapid surface crystallization of late-stage Fe-rich pyroxene, ilmenite, and plagioclase in the second stage of cooling of the sample. There is some scatter at higher Fe# and very little indication of a crystallization trend in 12030,187, which implies that ilmenite and plagioclase were late-stage, and cocrystallized rapidly in a surface lava flow.

Comparison Using Olivine Chemistry

It has been previously demonstrated by Fagan et al. (2013) (see also Alexander et al. 2014; Snape et al. 2014) that trace elements in olivine, and in particular Ti/V ratios, may be used to distinguish between some different Apollo 12 basalt groups. Olivine basalts have $Ti/V < 3$, whereas ilmenite basalts have $Ti/V > 3.5$. Pigeonite basalts overlap the other two suites and cannot be distinguished using this ratio (Fagan et al. 2013). Olivine in samples 889_2A, 8A, 12A, and 12030,187 and 12070,891 all have limited ranges of Sc concentrations and core Ti/V measurements <3, although rim measurements cover a wider range (Fig. 7). Sample 889_2A has distinct olivine chemistry with higher contents of the compatible elements Co, Mn, and Ni, which indicates a difference in the parent melt composition. These samples are therefore likely to be olivine or pigeonite basalts. Other samples with $Ti/V > 3.5$ in olivine cores are 889_1A (Ti/V 6–32) and 889_6A, which has the highest Ti/V ratios (Ti/V 13–55) as a result of low V content. Both of these samples are coarse-grained and sample 889_6A in particular is likely to be a cumulate. As equilibration temperatures control the amount of V in olivine, this method is unlikely to be as effective in distinguishing coarse-grained slowly cooled samples. V is compatible in olivine and decreases with crystallization while Ti is incompatible and increases, leading to the higher Ti/V ratios in the rims and more evolved olivine compositions (Fagan et al. 2013).

Comparison Using Ilmenite Chemistry

A solid solution exists between ilmenite ($FeTiO_3$) and geikielite ($MgTiO_3$). The composition reflects the magmatic chemistry (Papike et al. 1998) and, therefore, may provide a useful discriminator between basalt

types, since ilmenite compositions with the highest Mg content tend to come from high-Mg rocks (Papike et al. 1991). MgO content of ilmenite (see supporting information), appear to separate olivine basalts from the other basalt groups. Ilmenite compositions in pigeonite, ilmenite, and feldspathic basalts do not exceed 2 wt% MgO. Olivine cumulate 12070,889_6A has particularly high concentrations of MgO in ilmenite (approximately 5.3 wt%). It has equilibrated mafic phases, but unlike other similar samples which show equilibration in all phases, 12070,889_6A contains unequilibrated plagioclase with high Mg#, but a wide range of An content ($An_{86–91}$) and also high concentrations of trace elements in plagioclase compared with the other samples studied.

Comparison Using Plagioclase Chemistry

Plagioclase chemistry may also be useful for discriminating between lunar basalt types, especially in samples which do not contain olivine, or where ilmenite is too fine-grained for effective analysis of its MgO content. A plot of anorthite (An#) content against the Mg# of plagioclase (see supporting information Supplementary Note 3) can highlight chemical differences between samples. Most samples show an initial increase in An content as Mg# starts to decrease, followed by a steep decrease in Mg# at relatively consistent high An content, with An decreasing finally at low Mg# toward the end of crystallization. Olivine basalts have higher Mg# content in plagioclase that drop sharply with a relatively narrow range of An# content. Trends in 12070,889_6A remain anomalous with a wider range of An content, but less varied Mg# in plagioclase than other samples. The plagioclase crystallization trend for 12070,891 shows no obvious correlation between Mg# and An#. There is a range of An content but all are <90 and Mg# in plagioclase are low for all measurements. This indicates that plagioclase is a late-stage phase. No trend could be plotted for 12030,187 because the plagioclase is too fine-grained for effective analysis. The only analysis obtained from this sample has Mg# 5 at An# 91.

Many samples have plagioclase too fine grained to be analyzed by LA-ICP-MS, but where it has been possible, trace element concentrations and ratios are similar between the different basalt groups and do not appear to distinguish between them, although the scarcity of comparative mineral trace element data makes such comparisons challenging. Two samples from this study 12070,889_3A and 6A have higher levels of Eu (up to 12 ppm in 889_3A, and 11 ppm in 889_6A) and Ba (up to 290 ppm in 889_3A, and up to 225 ppm in 889_6A) and higher levels of Sr in plagioclase (up to 1324 ppm in 889_3A, and 1253 ppm in 889_6A) than other Apollo 12 basalts. The compositional range implies that the plagioclase crystals in these samples are not equilibrated, and in sample 12070,889_6A it is the only unequilibrated phase. Sample 889_3A is not similar to 889_6A, however, since it contains a range of pyroxene compositions indicating that the mafic phases are not equilibrated. Crystallization trends (Figs. 3 and 4) have suggested that plagioclase reached the liquidus at an earlier stage in this sample in comparison to others from the same sample set. This could explain why plagioclase contains higher concentrations of compatible elements while pyroxenes contain lower concentrations.

Investigating Likely Parent Lithologies

Comparison between the mineral chemistry of these samples and other Apollo 12 basalts can help to constrain their origin. As discussed in the Previously Identified Apollo 12 Basalt Suites section, Apollo 12 basalts are grouped into four suites of pigeonite, olivine, ilmenite, and feldspathic basalts (James and Wright 1972; Rhodes et al. 1977; Neal et al. 1994a). Where the mineral chemistry has shown that the sample is representative of the parent melt, for example, as a result of the effective recalculation of the Mg# of the melt, then the bulk chemistry has been used to provide an initial comparison to other Apollo 12 samples using a simple paired samples *t*-test to compare bulk oxide values (Table 4). This method is particularly useful for finer grained to vitrophyric samples such as 12030,187 and 12070,891. However, it is emphasized that this test is useful only in addition to mineral chemistries and chemical trends. Full details of the *t*-test method are given in the supporting information (Supplementary Note 4) accompanying this paper. Where samples are particularly coarse-grained (grainsize >0.6 mm), there are too few mineral phases present to effectively categorize the sample, and those phases which are present often exhibit signs of subsolidus equilibration. This represents a limitation in sample categorization based on mineral chemistry.

Olivine Basalts

Sample 12030,187 has a high modal abundance of olivine, and both modeled and measured bulk Mg# and Ti/V ratios in olivine indicate that it is likely to be an olivine basalt. The *t*-test indicates that this sample is chemically similar to Apollo 12 samples 12004 (*t*-test value 0.28), an olivine basalt, and 12009 (*t*-test value 0.34), an olivine vitrophyre. The texture is similar to that of lunar sample 12009, which also contains skeletal olivine and pyroxene in a groundmass of microcrystalline devitrified glass (McGee et al. 1977), with cryptocrystalline plagioclase. Pyroxene compositions in both 12004 and 12009 cover the same

Table 4. Proposed classification of samples based on results in this study. Classification is based on the mineral chemistry wherever possible, and where this has been shown to be representative then additional comparison of the bulk chemistry and texture has also been taken into account using statistical analysis of the bulk chemical oxides and comparison of mineral chemistry to give the closest possible match. Full details of the reasons for the characterization are detailed in the text. The *t*-test value is the statistic resulting from the paired samples *t*-test for the relevant sample against the comparable sample listed; the lower the value, the more similar the samples. Where the *t*-test value is greater than 1, the comparison is deemed unsuitable. Full details are given in supporting information Supplementary Note 4.

Sample	Preliminary site-specific classification	Most similar A12 sample	*t*-test value	See Note below
889_1A	Ilmenite basalt	12054	0.392	
889_2A	Pigeonite basalt	12011	0.327	
889_3A	n/a	12072	0.619	1
889_4A	Ilmenite basalt	12047	0.924	
889_6A	n/a	12005	1.222	2
889_7A	Ilmenite basalt	12016	0.527	
889_8A	Olivine basalt	12075	0.180	
889_9A	Pigeonite basalt	12031	0.606	
889_10A	n/a	n/a	Rejected	3
889_11A	Pigeonite basalt?	12031	1.672	4
889_12A	Olivine basalt	12053	0.692	
12070,891	Pigeonite basalt	12052	0.146	
12030,187	Olivine basalt	12004	0.285	

1. Too coarse grained with insufficient mineral phases for characterization.
2. Olivine cumulate based on mineral chemistry and relationships.
3. Too coarse grained with insufficient mineral phases for characterization.
4. Coarse grained but likely to be a pigeonite basalt from mineral chemistry.

range (Brett et al. 1971) with similar features, for example, sporadic pigeonite compositions in augite rims and a wide range of olivine compositions.

Sample 889_8A is very similar in terms of its bulk chemical properties to lunar samples 12075, 12014, and 12076 (*t*-test values 0.18, 0.22, and 0.25, respectively), which are all olivine basalts. The measured bulk Mg# of 54 and the predicted equilibrium melt Mg# from the olivine core measurements of Mg# 47 indicate that it is likely to be an olivine or ilmenite basalt, and the bulk chemical properties for 12075 are remarkably similar with <3% difference between all oxides other than Al_2O_3.

Sample 889_12A is relatively coarse grained but nevertheless contains olivine. The measured bulk Mg# is 49 which is too high for a pigeonite basalt; however, the predicted bulk Mg# from olivine cores is 45, which is on the borderline between all three basalt types and therefore inconclusive. Olivine cores have Ti/V < 3, which indicates that this is not an ilmenite basalt. This sample has identical mineral chemistries to 889_8A. Olivine chemistries are similar both in terms of major and trace elements, with maximum olivine Mg# of 72 in both samples and the same range of Mn, Co, Ni, and V contents (Fig. 7). MgO content in ilmenite are also similar (up to 2.6 wt% MgO in 889_8A, and up to 1.8 wt% in 889_12A, higher than all other samples with the exception of 889_6A).

Pigeonite Basalts

The bulk chemistry and modeled bulk Mg# from sample 12070,891, together with mineral compositions, indicate that it is likely to be a pigeonite basalt. The statistical *t*-test suggests that it is chemically similar to many other Apollo 12 pigeonite basalts but in particular to samples 12052, 12065, and 12053 (*t*-test values 0.15, 0.19, and 0.19, respectively). Texturally this sample is very similar to 12052 and 12053, which are both pigeonite basalts with hollow pigeonite cores exhibiting a sharp boundary and augite rims, in a fine-grained feathery groundmass (Kushiro and Haramura 1971; Papike et al. 1971). Pyroxene compositions cover the same range and show similar trends (Papike et al. 1971).

Sample 889_2A is similar in terms of its bulk chemistry to many other samples, most notably 12011 and 12065 (*t*-test value 0.33 for both samples), but these are pigeonite basalts, whereas 2A has a bulk Mg# 48 which suggests that it is more likely to be an olivine or an ilmenite basalt. However, the predicted equilibrium melt Mg# is 43 from the olivine compositions, indicating that it is more likely to be a pigeonite basalt.

Sample 889_9A is unlikely to be representative of its parent melt composition. The statistical tests indicate that it has some similarities with lunar sample 12031 (*t*-test value 0.61), a coarse-grained pigeonite basalt, originally thought to be a feldspathic basalt. Plagioclase compositions are similar in both these samples ($An_{86–94}$ for 12031, Beaty et al. 1979; $An_{84–91}$ in 889_9A).

Sample 889_11A is also coarse grained (grain size >0.6 mm). The sample has a narrow range of plagioclase An content (90–93) with high plagioclase Mg# (26–50, see supporting information). Crystallization trends are similar to 889_2A, 8A, and 12A, while MgO content in ilmenite are also similar to 889_2A. This could indicate that the sample is a fragment from a coarse-grained pigeonite basalt, which crystallized from an evolved melt.

Ilmenite Basalts

The *t*-test indicates that 889_1A is similar to Apollo 12 samples 12007 and 12054 (*t*-test values 0.32 and 0.39,

respectively) in terms of its bulk chemistry. Sample 12054 is a medium-grained equigranular ilmenite basalt (grain size approximately 0.4 mm; Rhodes et al. 1977; Neal et al. 1994a, 1994b). Ti/V ratios even in the cores of pyroxene in 889_1A indicate that this sample is an ilmenite basalt. Plagioclase compositions cover a wide range of An content, some of which overlap all three Apollo 12 basalt suites. The crystallization trend for plagioclase is different from many other Apollo 12 samples commencing at a lower Mg# of 35. This shows that plagioclase crystallization commenced later than in many other samples or that this sample crystallized from a more evolved melt as indicated by the pyroxene compositions (Fig. 2) and Fe# versus Ti# and Al/Ti trends in pyroxene (Figs. 3 and 4) as well as the high trace element abundances in pyroxene.

Sample 889_4A is another relatively coarse-grained fragment that may not be representative and olivine analyses could not be carried out, as there are only very small grains of intergrown fayalitic olivine in the mesostasis. The statistical *t*-test indicates that, from the bulk composition, the most similar samples are ilmenite basalts 12047 and 12056 (*t*-test values 0.92 and 1.02, respectively), and it is thus likely that 889_4A is a member of the ilmenite basalt group. Sample 889_7A is another coarse-grained rock similar in texture, and mineral and chemical trends to 889_4A. Statistical analysis indicates that it is most similar to the ilmenite basalts 12016 and 12045 in terms of its bulk chemical properties (*t*-test values 0.53 and 0.56, respectively); however, these samples both contain olivine, which 889_7A does not, although this could be sampling bias. As with 889_4A, 889_7A is likely to be an ilmenite basalt with chemical similarities to other members of that group. Samples 889_4A and 889_7A show similarities in texture, mineral chemistry, and crystallization trends, and are probably two fragments of the same sample that broke in transit from JSC. Plagioclase compositions and trends overlap, and pyroxene crystallization trends and chemistries are the same. Both samples have patches of Fe-rich mesostasis.

Anomalous Samples

Sample 889_3A (2 mm) is coarse grained (grain size >0.6 mm) and its analyzed bulk chemistry is unreliable as it is unlikely to represent its parent melt. An additional problem in categorizing this sample is that it lacks olivine, which would have been useful for comparison and could have been used to effectively model the bulk rock Mg#, which is a primary discriminator for these basalts. The mineral chemistry and crystallization trends indicate that slow cooling in this coarse-grained sample has led to some equilibration of the phases.

Sample 889_6A is distinct in terms of its texture, bulk sample, and mineral chemistry. Statistical *t*-test calculations indicate that no samples are similar to 889_6A in terms of their bulk chemistry, with the only one showing any similarities being 12005 (*t*-test value 1.22), a coarse-grained Apollo 12 basalt currently assigned to the ilmenite basalt group but which is considered by Neal et al. (1994a) as likely to be anomalous and unrepresentative. This sample is also similar to samples 12003,308_5A, 12003.311, and 12003,316 (Snape et al. 2014) in terms of its high Mg# in plagioclase and high MgO content in ilmenite. However, there are still significant chemical differences. The texture and mineral chemistry suggests that this sample is an olivine cumulate, with a coarse, granular texture and excess cumulate olivine, equilibration in the mafic silicates, and compositional variation seen only in the late-stage intercumulus plagioclase. Therefore, it is likely that this sample formed from crystal settling in a single thick flow.

Sample 889_10A is also coarse grained and unlikely to be representative of its parent flow. Pyroxene crystals only show Fe-rich compositions (Fe# 58–96) and crystallization trends are also all Fe-rich. Plagioclase crystals all have low Mg# (0–28) with a limited range of An content ($An_{84–88}$). It is likely that this sample represents a coarse late-stage mesostasis and, thus, it is impossible to categorize from its mineral assemblage.

CONCLUSIONS AND FURTHER WORK

We have presented new geochemical and petrological data for 11 basaltic chips from the lunar soil sample 12070_889, 1 chip from 12070,891, and 1 from 12030,187. Some of these samples have grain sizes >0.6 mm, which is comparable to the sample size. As a result, these samples are probably unrepresentative of their parent melts in terms of their bulk chemistry and modal mineralogy. However, we have demonstrated that using a combination of bulk chemical properties, together with major, minor, and trace element chemical components of individual minerals, and corresponding crystallization trends, it is possible to make accurate comparisons both between the samples in this batch and with other basalt samples from the Apollo 12 site. We conclude that it is, therefore, possible to derive information about the parent lava flows and source regions for these small, regolith-derived, basaltic chips.

This work indicates that, where the sample is fine-grained (i.e., grain sizes <0.3 mm) or vitrophyric, the bulk chemistry can still give an accurate representation for classification purposes provided that the distribution of phases is homogeneous. This can be checked by comparison of the mineral chemistry with that of other samples from the different basalt groups. Coarse-grained basalts (grain size >0.6 mm) require much

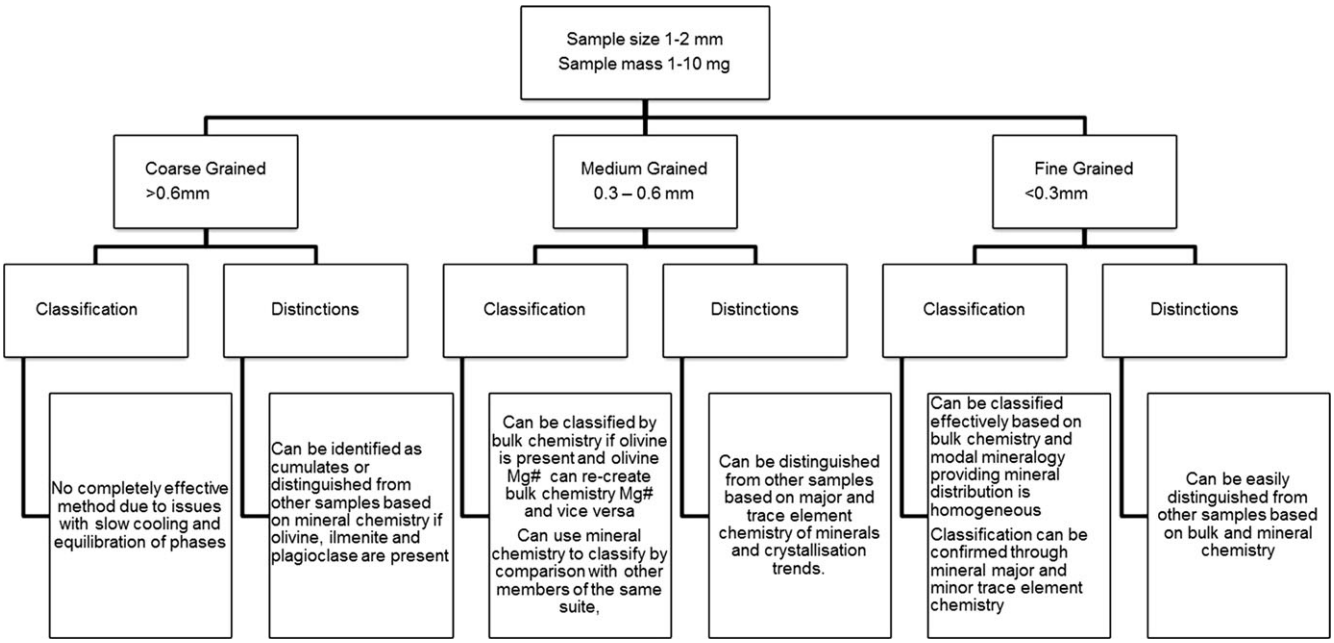

Fig. 10. Our proposed effective classification of small sample sizes. A flowchart summarizing when small-sized basalt samples can be classified within known mare basalt groups or distinguished from other types of samples, and the most effective nondestructive methods for achieving this.

larger sample sizes in order to achieve a representative analysis. Bulk rock Mg# is important for classification purposes within the classification scheme of Neal et al. (1994a). However, the bulk rock Mg# for samples of this size (approximately 2 mm) with crystal sizes >0.3 mm is unreliable on its own since the sample may not be representative of its parent melt. We have shown that where samples contain olivine, the equilibrium melt Mg# can be calculated, and trace elements can be compared to give an indication of the parent melt composition. We have also shown that it is possible to determine some differences between basalt groups from their ilmenite and plagioclase chemistry. This has allowed us make inferences regarding basaltic groupings in coarse-grained samples (grain size >0.6 mm) that do not contain olivine. Therefore, small samples of approximately 1 to 2 mm in size can be effectively categorized providing appropriate mineral phases (i.e., olivine, plagioclase, and ilmenite) are present. Where samples are fine grained, and representative, as demonstrated by recalculation of the parent melt Mg# or Ti#, then using a simple paired samples *t*-test can immediately provide a close match for the bulk chemical oxide measurements between a particular sample and other known basalt compositions. This is summarized in a flow chart (Fig. 10).

Of the 13 basaltic chips analyzed in this study, three belong to each of the previously identified olivine and ilmenite basalt suites, four to the pigeonite basalt suite, one is determined to be an olivine cumulate, and two are too coarse grained (with the grain size approaching the size of the sample) to contain sufficient mineral phases to make a determination (Table 4). Textural variation suggests that some of the samples could have originated at different depths within the same lava flow.

This paper presents results of the final part of a larger study (Alexander et al. 2014; Snape et al. 2014) of basaltic diversity at the Apollo 12 site, with a total of 40 basaltic fines analyzed. Of these, 15 have been categorized as olivine basalt chips, 1 as an olivine cumulate, 6 as ilmenite basalts, and 6 as pigeonite basalts. It had previously been suggested that three samples, 12023,155_4A and _5A (Alexander et al. 2014) and 12003,314_D (Snape et al. 2014), showed similarities to the feldspathic basalt 12038. However, additional analysis of the plagioclase chemistry of sample 12038 (see supporting information) indicates significant differences, and these samples are more likely to represent evolved pigeonite basalt compositions. Nine samples cannot be categorized and remain anomalous. Four of these samples are too coarse grained to make any meaningful interpretation because of the paucity of mineral phases in them, while the remaining five samples are likely to either be exotic to the Apollo 12 site or require a different melt composition at that site. Taken together, we find evidence for at least four, and possibly as many as six, parent lava flows at the Apollo 12 landing site, including the previously identified olivine, pigeonite, and ilmenite basalt classes and the potential feldspathic basalt class, together with material

potentially introduced from extraneous sources as a result of impact-related processes.

Finally, we note that the effective categorization and assessment of the petrographic relationships in small extraterrestrial samples based on mineral chemistry, as demonstrated here, will be important in the context of planned future sample return missions to the Moon, Mars, and asteroids because such missions are likely to return small sample masses that may present analytical challenges. Many of the major lunar science objectives outlined by the U.S. National Research Council (NRC) study in 2007 can only be addressed through further study of lunar samples (see Crawford and Joy [2014], and references therein). Future work on refining the methods presented here for analyzing and categorizing small, and potentially unrepresentative, samples will help to provide a basis for the way in which future samples can be categorized quickly and effectively to produce a more accurate understanding of the geology and magmatic history of sample-return sites.

Acknowledgments—We are grateful to CAPTEM for sample allocation and to the staff of the Lunar Sample Curation Facility at NASA JSC for their expert assistance in the selection and processing of these samples. We thank Dr. Andy Beard at Birkbeck for his assistance with electron microprobe techniques, and Dr. Martin Rittner, Birkbeck, for his assistance with using the LA-ICP-MS. We also thank Prof. Sara Russell and John Spratt at the Natural History Museum, London for assistance with electron microprobe techniques. We are also grateful to Dr. Adrian Jones, UCL, for useful petrology discussions. LA and IAC thank The Leverhulme Trust (grant RPG-2015-020) for financial support and KJ via STFC grant ST/M001253/1 and a Royal Society University Fellowship (RS/UF140190). We are grateful to Karl Cronberger (University of Notre Dame) for providing a calculator for pyroxene partition coefficients. We thank Drs. Cyrena Goodrich, Barbara Cohen, and Lydia Hallis for providing thoughtful advice on a previous version of this manuscript.

Editorial Handling—Dr. Cyrena Goodrich

REFERENCES

Alexander L., Snape J. F., Crawford I. A., Joy K. H., and Downes H. 2014. *S*earching for non-local lithologies in the Apollo 12 regolith: A geochemical and petrological study of basaltic coarse fines from the Apollo lunar soil sample 12023,155. *Meteoritics & Planetary Science* 49:1288–1304.

Anders E. and Grevesse N. 1989. Abundances of the elements: Meteoritic and solar. *Geochimica et Cosmochimica Acta* 53:97–214.

Arai T., Takeda H., and Warren P. H. 1996. Four lunar meteorites: Crystallization trends of pyroxenes and spinels. *Meteoritics & Planetary Science* 31:877–892.

Basaltic Volcanism Study Project. 1981. *Basaltic volcanism on the terrestrial planets*. New York: Pergamon Press, Inc. pp. 236–266.

Beaty D. W., Hill S. M. R., Albee A. L., and Baldridge W. S. 1979. Apollo 12 feldspathic basalts 12031, 12038 and 12072: Petrology, comparison and interpretations. Proceedings, 10th Lunar and Planetary Science Conference. pp. 115–139.

Borg L. E., Gaffney A. M., Shearer C. K., DePaolo D. J., Hutcheon I. D., Owens T. L., Ramon E., and Brennecka G. 2009. Mechanisms for incompatible-element enrichment on the Moon deduced from lunar basaltic meteorite Northwest Africa 032. *Geochimica et Cosmochimica Acta* 73:3963–3980.

Brett R., Butler P. J., Meyer C., Reid A. M., Takeda H., and Williams R. 1971. Apollo 12 igneous rocks 12004, 12008, 12009 and 12022: A mineralogical and petrological study. Proceedings, 2nd Lunar Science Conference. pp. 301–317.

Brown G. M., Emeleus C. H., Holland J. G., Peckett A., and Phillips R. 1971. Picrite basalts, ferrobasalts, feldspathic norites, and rhyolites in a strongly fractionated lunar crust. Proceedings, 2nd Lunar Science Conference. p. 583.

Cameron E. N. 1971. Opaque minerals in certain lunar rocks from Apollo 12. Proceedings, 2nd Lunar Science Conference. pp. 193–206.

Champness P. E., Dunham A. C., Gibb F. G. F., Giles H. N., MacKenzie W. S., Stumpfl E. F., and Zussman J. 1971. Mineralogy and petrology of some Apollo 12 samples. Proceedings, 2nd Lunar Science Conference. pp. 359–376.

Compston W., Berry H., Vernon M. J., Chappell B. W., and Kaye M. J. 1971. Rubidium-strontium chronology and chemistry of lunar material from the Ocean of Storms. Proceedings, 2nd Lunar Science Conference. pp. 1471–1485.

Crawford I. A. and Joy K. H. 2014. Lunar exploration: Opening a window into the history and evolution of the inner solar system. *Philosophical Transactions of the Royal Society of London* A372:20130315.

Crawford I. A., Fagents S. A., and Joy K. H. 2007. Full Moon exploration. *Astronomy and Geophysics* 48:18–21.

Dungan M. A. and Brown R. W. 1977. The petrology of the Apollo 12 ilmenite basalt suite. Proceedings, 8th Lunar Science Conference. pp. 1339–1381.

El Goresy A., Ramdohr P., and Taylor L. A. 1971. The opaque minerals in the lunar rocks from Oceanus Procellarum. Proceedings, 2nd Lunar Science Conference. p. 219.

Fagan A. L., Neal C. R., Simonetti A., Donohue P. H., and O'Sullivan K. M. 2013. Distinguishing between Apollo 14 impact melt and pristine mare basalt samples by geochemical and textural analyses of olivine. *Geochimica et Cosmochimica Acta* 106:429–445.

Gibb F. G. F., Stumpfl E. F., and Zussman J. 1970. Opaque minerals in an Apollo 12 rock. *Earth and Planetary Science Letters* 9:217–224.

Green D. H., Ringwood A. E., Ware N. G., Hibberson W. O., Major A., and Kiss E. 1971. Experimental petrology and petrogenesis of Apollo 12 basalts. Proceedings, 2nd Lunar Science Conference. pp. 601–615.

Grove T. L. and Vaniman D. T. 1978. *Experimental petrology of very low Ti/VLT/basalts. Mare Crisium: The view from*

Luna, vol 24. New York: Pergamon Press Inc. pp. 445–471.

Haggerty S. E. and Meyer H. O. A. 1970. Apollo 12: Opaque oxides. *Earth and Planetary Science Letters* 9:379–387.

Hallis L. J., Anand M., Greenwood R. C., Miller M. F., Franchi I. A., and Russell S. S. 2010. The oxygen isotope compostion, petrology and geochemistry of mare basalts: Evidence for large-scale compositional variation in the lunar mantle. *Geochimica et Cosmochimica Acta* 74:6885–6899.

Hallis L. J., Anand M., and Strekopytov S. 2014. Trace-element modelling of mare basalt parental melts: Implications for a heterogeneous lunar mantle. *Geochimica et Cosmochimica Acta* 134:289–316.

James O. B. and Wright T. L. 1972. Apollo 11 and 12 mare basalts and gabbros: Classification, compositional variations, and possible petrogenetic relations. *Geological Society of America bulletin* 83:2357–2382.

Jolliff B. L., Gillis J. J., Haskin L. A., Korotev R. L., and Wieczorek M. A. 2000. Major lunar crustal terranes: Surface expressions and crust-mantle origins. *Journal of Geophysical Research* 105:4197–4216.

Jolliff B. L., Shearer C. Jr., Gaddis L. R., Pieters C. M., Head J. W., Haruyama J., Jaumann R., Ohtake M., Osinski G., Papanastassiou D. A., and Petro N. E., and Moonrise Science Team. 2010. MoonRise: Sampling South Pole-Aitken Basin as a recorder of solar system events. American Geophysical Union, Fall Meeting, P43A-01.

Jones J. H. 1995. Experimental trace element partitioning rock physics and relationships. In *A handbook of physical constants*, edited by Clark S. P. Washington, D.C.: American Geophysical Union. pp. 74–104.

Joy K. H. 2013. Trace elements in lunar plagioclase as indicators of source lithology (abstract #1033). 44th Lunar and Planetary Science Conference. CD-ROM.

Joy K. H., Crawford I. A., Downes H., Russell S. S., and Kearsley A. T. 2006. A petrological, mineralogical, and chemical analysis of the lunar mare basalt meteorite La Paz Icefield 02205, 02224 and 02206. *Meteoritics & Planetary Science* 41:1003–1025.

Joy K. H., Crawford I. A., Anand M., Greenwood R. C., Franchi I. A., and Russell S. S. 2008. The petrology and geochemistry of Miller Range 05035: A new lunar gabbroic meteorite. *Geochimica et Cosmochimica Acta* 72:3822–3844.

Joy K. H., Crawford I. A., Russell S. S., and Kearsley A. T. 2010. Lunar meteorite regolith breccias: An in situ study of impact melt composition using LA-ICP-MS with implications for the composition of the lunar crust. *Meteoritics & Planetary Science* 45:917–946.

Karner J., Papike J. J., and Shearer C. K. 2006. Comparative planetary mineralogy: Pyroxene major- and minor-element chemistry and partitioning of vanadium between pyroxene and melt in planetary basalts. *American Mineralogist* 91:1574–1582.

Keil K., Prinz M., and Bunch T. E. 1971. Mineralogy, petrology and chemistry of some Apollo 12 samples. Proceedings, 2nd Lunar Planetary Science Conference. p. 319.

Korotev R. L., Jolliff B. L., and Zeigler R. A. 2000. The KREEP components of the Apollo 12 regolith (abstract #1363). 31st Lunar and Planetary Science Conference. CD-ROM.

Korotev R. L., Joliff B. L., Zeigler R. A., Seddio S. M., and Haskin L. A. 2011. Apollo 12 Revisited. *Geochimica et Cosmochimica Acta* 75:1540–1573.

Kushiro I. and Haramura H. 1971. Major element variation and possible source materials of Apollo 12 crystaline rocks. *Science* 171:1235–1237.

Longhi J. 1992. Experimental petrology and petrogenesis of mare volcanics. *Geochemica et Cosmochimica Acta* 56:2235–2251.

Longhi J., Walker D., and Hays J. F. 1978. The distribution of Fe and Mg between olivine and lunar basaltic liquids. *Geochimica et Cosmochimica Acta* 42:1545–1558.

Longhi J., Durand S. R., and Walker D. 2010. The pattern of Ni and Co abundances in lunar olivines. *Geochimica et Cosmochimica Acta* 74:784–798.

McGee P. E., Warner J. L., and Simonds C. H. 1977. *Introduction to the Apollo collections. Part 1: Lunar igneous rocks*. NASA STI/Recon Technical Report N 77: 22034.

McKay D. S., Morrison D. A., Clanton U. S., Ladle G. H., and Lindsay J. 1971. Apollo 12 soil and breccias. Proceedings, 2nd Lunar Science Conference. pp. 755–774.

Meyer J. C. 2011. Lunar Sample Compendium (http://curator.jsc.nasa.gov/lunar/compendium.cfm). Accessed August 16, 2015.

Mitrofanov I. G., Zelenyi L. M., and Tret'yakov V. I. 2012. Upgraded program of Russian lunar landers: Studying of lunar poles. *Proceedings of the Annual Meeting of the Lunar Exploration Analysis Group*. LPI contribution 1685. Houston, Texas: Lunar and Planetary Institute. p. 3025.

Morris R. V. 1978. The surface exposure (maturity) of lunar soils: Some concepts and Is/FeO compilation. Proceedings, 9th Lunar and Planetary Science Conference. pp. 2287–2297.

Neal C. R. and Taylor L. A. 1992. Petrogenesis of mare basalts: A record of lunar volcanism. *Geochimica et Cosmochimica Acta* 56:2177–2211.

Neal C. R., Hacker M. D., Snyder G. A., Taylor L. A., Liu Y.-G., and Schmitt R. A. 1994a. Basalt generation at the Apollo 12 site, Part 1: New data, classification, and re-evaluation. *Meteoritics* 29:334–348.

Neal C. R., Hacker M. D., Snyder G. A., Taylor L. A., Liu Y.-G., and Schmitt R. A. 1994b. Basalt generation at the Apollo 12 site, Part 2: Source heterogeneity, multiple melts, and crustal contamination. *Meteoritics* 29:349–361.

Nyquist L. E. and Shih C.-Y. 1992. The isotopic record of lunar volcanism. *Geochimica et Cosmochimica Acta* 56:2213–2234.

Nyquist L. E., Bansal B. M., Wooden J. L., and Wiesmann H. 1977. Sr-isotopic constraints on the petrogenesis of Apollo 12 mare basalts (abstract). 8th Lunar and Planetary Science Conference. pp. 1383–1415.

Nyquist L. E., Shih C.-Y., Wooden J. L., Bansal B. M., and Wiesmann H. 1979. The Sr and Nd isotopic record of Apollo 12 basalts: Implications for lunar geochemical evolution. Proceedings, 10th Lunar and Planetary Science Conference. pp. 77–114.

Nyquist L. E., Wooden J. L., Shih C.-Y., Wiesmann H., and Bansal B. M. 1981. Isotopic and REE studies of lunar basalt 12038: Implications for petrogenesis of aluminous mare basalts. *Earth and Planetary Science Letters* 55:335–355.

Papanastassiou D. A., and Wasserburg G. J. 1971. Lunar chronology and evolution from Rb-Sr studies of Apollo 11 and 12 samples. *Earth and Planetary Science Letters* 11:37–62.

Papike J. J., Bence A. E., Brown G. E., Prewitt C. T., and Wu C. H. 1971. Apollo 12 clinopyroxenes: Exsolution and epitaxy. *Earth and Planetary Science Letters* 10:307–315.

Papike J. J., Hodges F. N., Bence A. E., Cameron M., and Rhodes J. M. 1976. Mare basalts: Crystal chemistry, mineralogy and petrology. *Reviews of Geophysics and Space Physics* 14:475–540.

Papike J., Taylor L., and Simon S. 1991. Lunar minerals. In *Lunar sourcebook*, edited by Heiken G. H., Vaniman D. T., and French B. M. Cambridge: Cambridge University Press. pp. 121–181.

Papike J. J., Ryder G., and Shearer C. K. 1998. Lunar samples. In *Planetary minerals*, edited by Papike J. J. Reviews in Mineralogy, vol. 36. Washington, D.C.: Mineralogical Society of America. pp. 5-1–5-234.

Pearce N. J. G., Perkins W. T., Westgate J. A., Gorton M. P., Jackson S. E., Neal C. R., and Chenery S. P. 1997. A compilation of new and published major and trace element data for NIST SRM 610 and NIST SRM 612 glass reference materials. *Geostandards Newsletter, The Journal of Geostandards and Geoanalysis* 21:115–144.

Reid J. B. 1971. Apollo 12 spinels as petrogenetic indicators. *Earth and Planetary Science Letters* 10:351–356.

Rhodes J. M., Wiesmann H., Rodgers K. V., Brannon J. C., Bansal B. M., and Hubbard N. J. 1976. Chemistry, classification, and petrogenesis of Apollo 17 mare basalts (abstract). 7th Lunar and Planetary Science Conference. pp. 1467–1489.

Rhodes J. M., Blanchard D. P., Dungan M. A., Brannon J. C., and Rodgers K. V. 1977. Chemistry of Apollo 12 mare basalts: Magma types and fractionation processes. Proceedings, 8th Lunar Science Conference. pp. 1305–1338.

Roeder P. L. and Emslie R. F. 1970. Olivine-liquid equilibrium. *Contributions to Mineralogy and Petrology* 29:275.

Schnare D. W., Day J. M. D., Norman M. D., Liu Y., and Taylor L. A. 2008. A laser-ablation ICP-MS study of Apollo 15 low-titanium olivine-normative and quartz-normative mare basalts. *Geochimica et Cosmochimica Acta* 72:2556–2572.

Shearer C. K. and Papike J. J. 2005. Early crustal building processes on the Moon: Models for the petrogenesis of the magnesian suite. *Geochimica et Cosmochimica Acta* 69:3445–3461.

Shearer C. K., Hess P. C., Wieczorek M. A., Pritchard M. E., Parmentier E. M., Borg L. E., Longhi J., Elkins-Tanton L. T ., Neal C. R., Antonenko I., Canup R. M., Halliday A. N., Grove T. L., Hager B. H., Lee D.-C., and Wiechert U. 2006. In *Thermal and magmatic evolution of the Moon*, edited by Joliff B. L., Wieczorek M. A., Shearer C. K. and Neal C. R. *New views of the Moon*, Reviews in mineralogy and geochemistry, vol. 60. Washington, D.C.: Mineralogical Society of America. pp. 365–469.

Snape J. F., Beaumont S., Burgess R., Crawford I. A., and Joy K. H. 2011a. An evaluation of techniques used in the age and petrologic analysis of Apollo 12 basalts (abstract #2011). 42nd Lunar and Planetary Science Conference. CD-ROM.

Snape J. F., Joy K. H., and Crawford I. A. 2011b. Characterization of multiple lithologies within the lunar feldspathic regolith breccia meteorite Northeast Africa 001. *Meteoritics & Planetary Science* 46:1288–1312.

Snape J. F., Alexander L., Crawford I. A. C., and Joy K. H. 2013. Basaltic regolith sample 12003,314: A new member of the Apollo 12 feldspathic basalt suite? (abstract #1044). 44th Lunar and Planetary Science Conference. CD-ROM.

Snape J. F., Joy K. H., Crawford I. A., and Alexander L. 2014. Basaltic diversity at the Apollo 12 site: Inferences from petrologic examinations of the soil sample 12003. *Meteoritics & Planetary Science*, 49:842–871.

Snyder G. A., Neal C. R., Taylor L. A., and Halliday A. N. 1997. Anatexis of lunar cumulate mantle in time and space: Clues from trace-element, strontium, and neodymium isotopic chemistry of parental Apollo 12 basalts. *Geochimica et Cosmochimica Acta* 61:2731–2747.

Stöffler D., Ryder G., Ivanov B. A., Ivanov N. A., Cintala M. J., and Grieve R. A. F. 2006. Cratering history and lunar chronology. In *New views of the Moon*, edited by Joliff B. L., Wieczorek M. A., Shearer C. K., and Neal C. R. Reviews in Mineralogy and Geochemistry, vol. 60. Washington, D.C.: Mineralogical Society of America. pp. 519–596.

Sun C. and Liang Y. 2012. Distribution of REE between clinopyroxene and basaltic melt along a mantle adiabat: Effects of major element composition, water, and temperature. *Contributions to Mineralogy and Petrology* 163:807–823.

Sun C. and Liang Y. 2013. Distribution of REE and HFSE between low-Ca pyroxene and lunar picritic melts around multiple saturation points. *Geochimica et Cosmochimica Acta* 119:340–358.

Taylor L. A., Kullerud G., and Bryan W. B. 1971. Opaque mineralogy and textural features of Apollo 12 samples and a comparison with Apollo 11 rocks. Proceedings, 2nd Lunar Science Conference. pp. 855–871.

Wakita H. and Schmitt R. A. 1971. Bulk elemental composition of Apollo 12 samples: Five igneous and one breccias rocks and four soils. Proceedings, 2nd Lunar Science Conference. pp. 1231–1236.

Walker D., Kirkpatrick R. J., Longhi J., and Hays J. F. 1976a. Crystallization history of lunar picritic basalt sample 12002—Phase-equilibria and cooling-rate studies. *Geological Society of America Bulletin* 87:646–656.

Walker D., Hays J. F., Longhi J., and Kirkpatrick R. J. 1976b. Differentiation of an Apollo 12 picrite magma. Proceedings, 7th Lunar Science Conference. pp. 1365–1389.

Warren P. H. 1997. The unequal host-phase density effect in electron probe defocused beam analysis: An easily correctable problem (abstract #1497). 28th Lunar and Planetary Science Conference. CD-ROM.

Weill D. F., Grieve R. A., McCallum I. S., and Bottinga Y. 1971. Mineralogy-petrology of lunar samples. Microprobe studies of samples 12021 and 12022; viscosity of melts of selected lunar compositions. Proceedings, 2nd Lunar Science Conference. p. 413.

Willis J. P., Ahrens L. H., Danchin R. V., Erlank A. J., Gurney J. J., Hofmeyr P. K., McCarthy T. S., and Orren M. J. 1971. Some interelement relationships between lunar rocks and fines, and stony meteorites. Proceedings, 2nd Lunar Science Conference. pp. 1123–1138.

Zeigler R. A., Korotev R. L. and Jolliff B. L. 2012. Pairing relationships among feldspathic lunar meteorites from Miller Range. Antarctica (abstract #2377). 43rd Lunar and Planetary Science Conference Abstract. CD-ROM.

Zolensky M. E., Pieters C., Clark B., and Papike J. J. 2000. Small is beautiful: The analysis of nanogram-sized astromaterials. *Meteoritics & Planetary Science* 35:9–29.

SUPPORTING INFORMATION

Additional supporting information may be found in the online version of this article:

Appendix S1. Electronic data appendix.

Supplementary Note 1. The Apollo 12 Landing site.

Supplementary Note 2. Additional images of basalt samples.

Supplementary Note 3. Additional data chemistry plots.

Supplementary Note 4. Statistical analyses of bulk chemical oxides.